Physica D 41 (1990) 403–449
North-Holland

AMPLITUDE RESPONSE OF COUPLED OSCILLATORS*

D.G. ARONSON
School of Mathematics, University of Minnesota, Minneapolis, MN 55455, USA

G.B. ERMENTROUT
Department of Mathematics, University of Pittsburgh, Pittsburgh, PA 15260, USA

and

N. KOPELL
Department of Mathematics, Boston University, Boston, MA 02215, USA

Received 1 August 1988
Revised manuscript received 12 June 1989
Accepted 13 June 1989
Communicated by J.E. Marsden

We investigate the interaction of a pair of weakly nonlinear oscillators (e.g. each near a Hopf bifurcation) when the coupling strength is comparable to the attraction of the limit cycles. Changes in amplitude cannot then be ignored, and there are new phenomena. We show that even for simple forms of these equations, there are parameter regimes in which the interaction causes the system to stop oscillating, and the rest state at zero, stabilized by the interaction, is the only stable solution. When the uncoupled oscillators have a local frequency that is independent of amplitude (zero shear), and the coupling is scalar, we give a complete description of the behavior. We then analyze more complicated equations to show the effects of amplitude-dependent frequency in the uncoupled equations (nonzero shear) and nonscalar coupling. For example, when there is shear, there can be bistability between a phase-locked solution and an unlocked "drift" solution, in which the oscillators go at different average frequencies. There can also be bistability between a phase locked solution and an equilibrium, nonoscillatory, solution. The equations for the zero shear case have a pair of degenerate bifurcation points, and the new phenomena in the nonzero shear case arise from a partial unfolding of these singularities. When the coupling is nonscalar, there are a variety of new behaviors, including bistability of an in-phase and an anti-phase solution for two identical oscillators, parameters for which only the anti-phase solution is stable, and "phase-trapping," i.e., nonlocked solutions in which the oscillators still have the same average frequency. It is shown that whether the coupling is diffusive or direct has many effects on the behavior of the system.

1. Introduction

There have been many recent articles on the behavior of forced and coupled oscillators with applications in biology and chemistry [1–20]. Many of these consider only "phase effects" [4–6, 8–10, 12, 14, 16]. That is, they deal with limit cycle oscillations having a stable periodic solution and ignore all coordinates other than the one that parameterizes the limit cycle. This approach can be justified by invariant manifold theory (see, e.g., Fenichel [21]) if the attraction to the limit cycle is "strong" compared to the amplitude of the forcing or coupling. For example, weak coupling has been exploited in many examples to analyze

*Research partially supported by the NSF under grants DMS 8796235, DMS 8701405 and DMS 8301247, and by the AFOSR under URI contract F49620-86-C-0131 to Northeastern University.

phenomena such as phase locking and "phase drift" [4, 5, 8–10, 12, 14]. The major advantage of this simplification is that complicated systems of differential equations can be reduced to flows on a much lower-dimensional phase space, namely an invariant torus having only one dimension per oscillator.

If the coupling is strong or the attraction to the limit cycle is not large compared to coupling strength, then many new phenomena can occur. Most of our knowledge of this comes from numerical simulations and asymptotic methods. For example, Bar-Eli [3] has recently studied the behavior of two diffusively and linearly coupled oscillators governed by equations

$$\begin{aligned} \mathrm{d}X_1/\mathrm{d}t &= F_1(X_1) + D_1(X_2 - X_1), \\ \mathrm{d}X_2/\mathrm{d}t &= F_2(X_2) + D_2(X_1 - X_2), \quad X_1, X_2 \in \mathbb{R}^n \end{aligned} \tag{1.1}$$

for a variety of different oscillators F_i, and coupling with $D_1 = D_2 = dI$, where I is the identity matrix, and d is a scalar. (We call this scalar coupling.) He uses numerical methods to show that, if F_1 and F_2 are sufficiently different, then for a range of values of d, coupling causes the system to stop oscillating and stabilize at a constant steady state. Models describing only phase cannot explain this coupling-induced oscillator death, which we shall refer to as the *Bar-Eli effect*, since the stable steady state is far from any limit cycles of the system. Our objective in this paper is to show that the Bar-Eli effect occurs generically in a broad class of systems (1.1) when the individual oscillators are near a supercritical Hopf bifurcation, and to show how the Bar-Eli effect fits into the global dynamics of such systems.

Other examples of phenomena which cannot be explained in terms of phase alone occur in the work of Schreiber and Marek [22], who consider (1.1) in the case of identical oscillators ($F_1 = F_2$) with identical nonscalar coupling ($D_1 = D_2 \neq dI$). Numerically, they find various tori, multiple oscillations, period doublings and chaos for large enough coupling strengths. Most of the present paper is devoted to the scalar coupling case, but we do treat nonscalar coupling briefly in section 5. In a recent paper [1] Aronson et al. have studied a pair of identical coupled oscillators with certain symmetries and found complicated patterns in the stability behavior of the out-of-phase solutions. Both amplitude and phase are needed in their analysis.

An important instance where the attraction to a limit cycle is not "strong" is near a Hopf bifurcation point. In this case, the attraction to the limit cycle is proportional to the distance from criticality. If we assume that such systems are coupled with strength of the same magnitude, it is no longer possible to assume that the trajectories of the system stay in a small neighborhood of the limit cycle. However, because a system near Hopf bifurcation is only weakly nonlinear, the introduction of polar coordinates is still useful and gives information about the behavior of amplitude as well as phase. In this paper, we will study the effects of coupling on systems near a Hopf bifurcation.

We shall *not* assume that the oscillators are identical; indeed, we shall study the effects of differences in the natural frequencies on the amplitude of the output of the coupled system. We do assume that the coupling is symmetric, i.e. $D_1 = D_2$. We will derive a system of differential equations which govern the amplitude and phase of the oscillations. From these equations we are able to study the Bar-Eli effect and its role in the global dynamics of our coupled system. We begin with a local result for families of systems parameterized by coupling strength with all other parameters held fixed. Roughly speaking, we show that if the oscillators are sufficiently different then the Bar-Eli effect occurs, i.e., the amplitude of the stable solution is zero for some range of the parameter. However, oscillator death does not occur if the oscillators are sufficiently similar. We next study the global dynamics to determine the long-time behavior of the system in various regions of the parameter space. We show that for some values of the parameters there is bistability, with a stable phase-locked solution coexisting with a more complicated, but stable, drift

solution (see below) or with a nonoscillatory equilibrium solution. Such bistability has been found for forced oscillators [23] but not, to our knowledge, for a pair of equally coupled oscillators. If the coupling matrix D is not scalar, the bifurcation diagram can be very complicated, as we show by analysis and numerical simulations. See also ref. [24].

The equations we shall study are derived as approximate equations from (1.1), and variations of it, under some simplifying assumptions when the uncoupled oscillators $\mathrm{d}X_i/\mathrm{d}t = F_i(X_i)$ are near Hopf bifurcations. The deviations and the assumptions are spelled out in the appendix. If the coupling is scalar, then to lowest order the resulting equations have the form

$$\begin{aligned}
\dot{r}_1 &= r_1\left(1 - \kappa\gamma - r_1^2\right) + r_2\gamma\cos\phi, \\
\dot{r}_2 &= r_2\left(1 - \kappa\gamma - r_2^2\right) + r_1\gamma\cos\phi, \\
\dot{\phi} &= \Delta + q_1 r_1^2 - q_2 r_2^2 - \gamma\left(\frac{r_1}{r_2} + \frac{r_2}{r_1}\right)\sin\phi.
\end{aligned} \tag{1.2}$$

We also study oscillators coupled in a non-scalar manner.

In (1.2), the r_i are amplitudes measured in the planes of the Hopf bifurcations and $\phi \equiv \theta_2 - \theta_1$, where the θ_i are the angular variables in those planes. Note that the dynamics depend on the phases θ_1 and θ_2 only through ϕ to lowest order in the relevant perturbation variable. This is a consequence of being near the Hopf bifurcation. The parameters γ and κ arise through coupling interactions of the oscillators, which has been assumed to be scalar. When $\kappa = 1$ the interaction is "diffusive" as in (1.1), while $\kappa = 0$ corresponds to "direct" coupling, with $X_2 - X_1$ replaced by X_2 in the first equation, and $X_1 - X_2$ replaced by X_1 in the second equation. We assume that the rates of attraction of each oscillator to its limit cycle in the absence of coupling are equal. The terms involving the q_i are related to "shear"; if they are set to zero, then the uncoupled oscillators reduce to what are known as radial isochronal clocks [10]. That is, all trajectories that start at the same value of ϕ go to the same asymptotic phase. If q_1 and q_2 are nonzero, the lines of constant asymptotic phase (which are radii if $q_j = 0$) are twisted [10, 17, 20], and the local frequency depends on the local amplitude. The parameter Δ, given by

$$\Delta \equiv \omega_2 - \omega_1 + q_2 - q_1,$$

measures a relevant difference between the oscillators, where ω_j is the natural frequency of the jth oscillator at its Hopf bifurcation.

Equilibria of (1.2) correspond to periodic solutions of (1.1). For such solutions, in which the phase difference ϕ is constant, two oscillators are said to be *phase locked*. There are two types of nonequilibrium solutions of interest for (1.2). One type we shall consider is *phase-drift* solutions. As in equations which depend only on phases and not on amplitudes, phase-drift refers to solutions for which the phase difference moves through all phases, so that the oscillators behave almost as if they were uncoupled. This phenomenon has been studied for phase models by many authors [9, 12, 15, 16] and has also been called phase slipping, frequency pulling, and phase walkthrough.

The other kind of nonequilibrium solution to (1.2) of interest is sometimes called a *phase-trapped* solution. It is a solution periodic in both r_j and ϕ, i.e., one for which there is a T such that

$$r_j(t+T) = r_j(t), \qquad \phi(t+T) = \phi(t). \tag{1.3}$$

We note that the distinction between phase locking and phase trapping makes strict sense only for equations such as (1.2), which depend on $\theta_2 - \theta_1$, but not on the θ_i separately. In the full equations (1.1),

for which (1.2) represents a first-order approximation, the periodic solutions corresponding to constant ϕ in (1.2) do not necessarily have $\theta_2 - \theta_1$ independent of time (only independent to lowest order).

In section 2 we consider eq. (1.2) written in complex coordinates

$$z_j = r_j e^{i\theta_j}$$

and do the local analysis of the stability of the rest state at the origin $z_1 = z_2 = 0$. Since the shear parameters q_j affect only quadratic terms, they play no role in the linear analysis near the origin. Thus the only relevant parameters are the coupling parameters γ and κ, and the difference parameter Δ. We show that the *Bar-Eli effect occurs if and only if* $|\Delta| > 2/\kappa$. Note, in particular, that the Bar-Eli effect cannot occur in the direct coupling case $\kappa = 0$.

In section 3 we examine the global dynamics of the system (1.2) with $\kappa = 1$ in the absence of shear terms. The analysis is aided by a fortuitous connection to the work of Aronson et al. [1], in which certain equations relevant to this paper occur in a somewhat different context. That work enables us to divide the parameter half plane $\{(\gamma, \Delta)$: $\gamma \in (0, \infty), \Delta \in \mathbb{R}\}$ into three *disjoint* open regions as shown in fig. 4. In one of these regions (characterized by relatively small γ) there exists a unique asymptotically stable phase-drift solution (i.e., a phase drift with $r_1 = r_2$). These phase-drift solutions fill out an invariant torus as in the purely phase models. In another of these regions (characterized by relatively large γ), there exists a unique asymptotically stable phase-locked solution. In the remainder of the parameter half plane we have the Bar-Eli effect, i.e. the origin is asymptotically stable and every other trajectory is attracted to it.

The transitions between the regions described above occur along bifurcation curves (fig. 4) which (for $\kappa = 1$) intersect at two highly degenerate bifurcation points $(\gamma, \Delta) = (1, \pm 2)$. Nonzero shear terms in (1.2) partially unfold these points with the result that the various behavior regions in the parameter half plane are no longer disjoint, i.e. there are now *parameter regions where the system is bistable*. As a consequence, the bifurcation diagram in the nonzero shear case (fig. 15) is considerably more complicated than the diagram for zero shear (fig. 4). However, note that the region where the Bar-Eli effect occurs remains unchanged.

The unfoldings of the points $(1, \pm 2)$ depend on the sign of $\nu \equiv q_2 - q_1$. Throughout this work we shall assume, without loss of generality, that $\nu \geq 0$. With this convention, we show in section 4 that the unfolding of the point $(1,2)$ for $\nu > 0$ always contains a degenerate saddle–node (Bogdanov–Takens point). This local information together with some global properties of our particular system (1.2) allows us to show (in section 4) the existence of an open set in the parameter space where stable phase drift and stable phase lock coexist. The separatrix between these two stable trajectories is an unstable phase-trap solution which results from Hopf bifurcation associated with the Bogdanov–Takens point. The unfolding of the point $(1, -2)$ for $\nu > 0$ is simpler and leads to the existence of an open parameter set in which stable phase lock coexists with either stable phase drift or stable rest. The details in fig. 15 are obtained by combining analytic and numerical information.

The frequency of the coupled system depends, through the amplitudes, on the shear terms, and this leads to some results about how coupling can change the output frequency. It will be seen that diffusive and direct coupling have different effects on the frequency of the locked system, essentially because of their different effects on the amplitudes.

In section 5, we turn to the case of nonscalar coupling, for which the equations are somewhat more complicated than (1.2). Even when $\Delta = 0$, the behavior of this system is quite complex. We show various transitions to stable phase-trapping and multiple stable phase locked states. Related papers have been written by Rand and Holmes [15], Linkens [13], Kawato and Suzuki [11], Schreiber and Marek [22], and

Aronson et al. [1]; some of these are discussed more below. More detailed work on another special case of these equations, with nonscalar coupling, was done by Chakraborty and Rand [24].

2. Stability of the rest state at zero

In this section, we show that the parameter Δ, which measures the difference in frequency and shear between the oscillators, has major effects on the amplitude of the coupled system. Specifically, we look at the trivial solution $r_1 = r_2 = 0$ and prove that, if $|\Delta| > \lambda/\kappa$, there is an interval of coupling strengths where the coupling can cause the rest state, which is unstable in the absence of coupling, to become stable. This is, in a sense, an effect inverse to examples in the work of Smale [18] and Turing [25], in which two systems, each with a stable rest point, can oscillate when coupled. (Also see refs. [26, 27] for another mechanism in which two oscillators, when coupled, can go to a stable steady state.) Like Bar-Eli, who demonstrated a similar stabilization effect numerically [3], we assume here that the coupling is scalar. (This assumption is incorporated in (1.2).) Our main result is a necessary and sufficient condition for the occurrence of the Bar-Eli effect (proposition 2.1).

To show that coupling can stabilize the rest state $r_1 = r_2 = 0$ it is convenient to work with the full four-dimensional system. As shown in the appendix, under some simplifying conditions, the system (1.2) is equivalent to

$$\begin{aligned} \dot{z}_1 &= z_1[1 + \mathrm{i}(\omega_1 + q_1) - (1 + \mathrm{i}q_1) z_1 \bar{z}_1] + \gamma(z_2 - \kappa z_1), \\ \dot{z}_2 &= z_2[1 + \mathrm{i}(\omega_2 + q_2) - (1 + \mathrm{i}q_2) z_2 \bar{z}_2] + \gamma(z_1 - \kappa z_2), \end{aligned} \tag{2.1}$$

where $z_j = r_j \exp(i\theta_j)$ for $j = 1$ and 2. Let $F(z_1, z_2)$ denote the right-hand side of (2.1). The differential of F at the origin, written as a linear operator on $\mathbb{R}^4$, is given by

$$DF(0,0) = \begin{pmatrix} 1 - \kappa\gamma & -(\omega_1 + q_1) & \gamma & 0 \\ \omega_1 + q_1 & 1 - \kappa\gamma & 0 & \gamma \\ \gamma & 0 & 1 - \kappa\gamma & -(\omega_2 + q_2) \\ 0 & \gamma & \omega_2 + q_2 & 1 - \kappa\gamma \end{pmatrix}.$$

If λ is an eigenvalue of $DF(0,0)$ and $p \equiv \lambda - (1 - \kappa\gamma)$, then p satisfies

$$p^4 - \left[2\gamma^2 - (\omega_1 + q_1)^2 - (\omega_2 + q_2)^2\right] p^2 + (\omega_1 + q_1)^2 (\omega_2 + q_2)^2 + 2\gamma^2 (\omega_1 + q_1)(\omega_2 + q_2) + \gamma^4 = 0.$$

This equation can be rewritten as

$$\left\{ p^2 - \left[\gamma^2 + (\omega_1 + q_1)(\omega_2 + q_2)\right] \right\}^2 = -(\omega_1 + \omega_2 + q_1 + q_2)^2 p^2,$$

from which we find

$$\lambda = 1 - \kappa\gamma \pm \sqrt{\gamma^2 - \tfrac{1}{4}\Delta^2} \pm \mathrm{i}\bar{\omega}, \tag{2.2}$$

where $\Delta = \omega_2 - \omega_1 + q_2 - q_1$ and $\bar{\omega} = \frac{1}{2}(\omega_1 + \omega_2 + q_1 + q_2)$.

The stability properties of the rest state at the origin and bifurcations from it are determined by the real parts of the eigenvalues λ of $DF(0,0)$. Let

$$L \equiv \mathrm{Re}\left(1 - \kappa\gamma + \sqrt{\gamma^2 - \tfrac{1}{4}\Delta^2} \pm i\bar{\omega}\right) = 1 - \kappa\gamma \qquad \text{for } \gamma \in [0, \tfrac{1}{2}|\Delta|],$$

$$= 1 - \kappa\gamma + \sqrt{\gamma^2 - \tfrac{1}{4}\Delta^2} \qquad \text{for } \gamma \in (\tfrac{1}{2}|\Delta|, \infty),$$

and

$$l \equiv \mathrm{Re}\left(1 - \kappa\gamma - \sqrt{\gamma^2 - \tfrac{1}{4}\Delta^2} \pm i\bar{\omega}\right) = 1 - \kappa\gamma \qquad \text{for } \gamma \in [0, \tfrac{1}{2}|\Delta|],$$

$$= 1 - \kappa\gamma - \sqrt{\gamma^2 - \tfrac{1}{4}\Delta^2} \qquad \text{for } \gamma \in (\tfrac{1}{2}|\Delta|, \infty).$$

Observe that L and l can change sign only when $\gamma = 1/\kappa$ or when γ satisfies

$$\sqrt{\gamma^2 - \tfrac{1}{4}\Delta^2} = |1 - \kappa\gamma|.$$

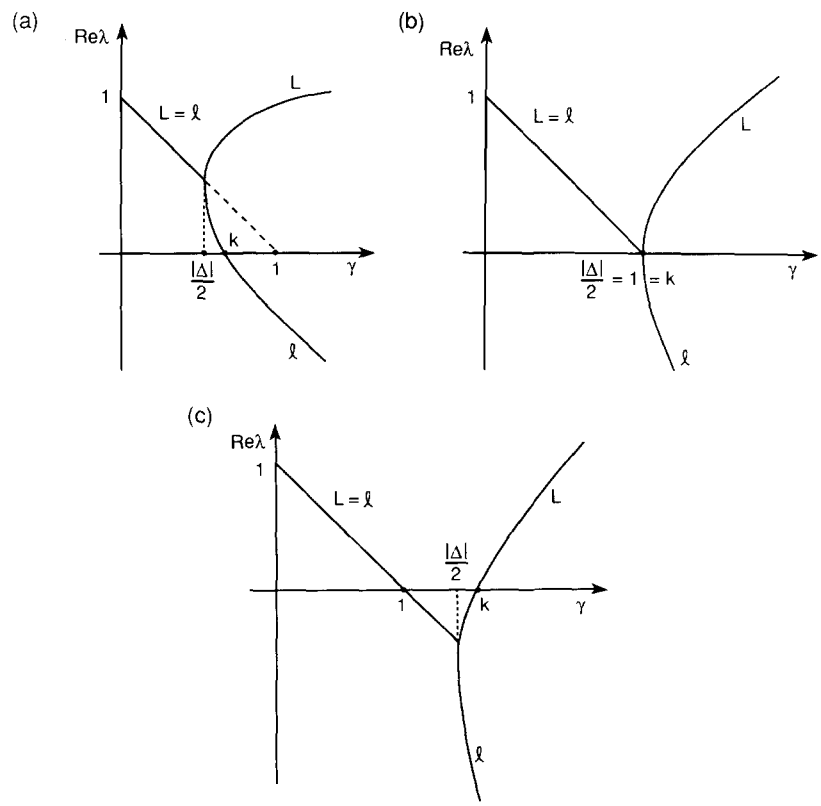

Fig. 1. Re λ, as defined in (2.2), versus coupling strength λ for (a) $\frac{1}{2}|\Delta| < 1$, (b) $\frac{1}{2}|\Delta| = 1$, (c) $\frac{1}{2}|\Delta| > 1$. Note that only in case (c) is there a range of γ for which the real parts of the eigenvalues are negative.

The latter equation has a unique positive solution given by

$$\gamma = k(\kappa, \Delta) \equiv \left[1/(1-\kappa^2)\right]\left(\sqrt{1+\tfrac{1}{4}(1-\kappa^2)\Delta^2} - \kappa\right) \quad \text{for } \kappa \in [0,1),$$
$$\equiv \tfrac{1}{2}\left(1+\tfrac{1}{4}\Delta^2\right) \quad \text{for } \kappa = 1.$$

It is not difficult to verify that $k(\cdot, \Delta)$ is continuous on $[0,1]$ and that $k(\kappa, \Delta) \geq \frac{1}{2}|\Delta|$ with equality if and only if $\kappa = 2/|\Delta|$.

Proposition 2.1

(a) If $1/\kappa < \frac{1}{2}|\Delta|$ then the rest state at the origin is asymptotically stable if $\gamma \in (1/\kappa, k)$ and unstable if $\gamma \in [0, 1/\kappa) \cup (k, \infty)$.

(b) If $1/\kappa \geq \frac{1}{2}|\Delta|$ then the rest is unstable for all $\gamma \in [0, \infty)$ except possibly $\gamma = \frac{1}{2}|\Delta|$ in case $\kappa = 2/|\Delta|$.

(c) Bifurcations occur at $\gamma = 1/\kappa$ and $\gamma = k$ for $1/\kappa < \frac{1}{2}|\Delta|$ and at $\gamma = k$ for $1/\kappa \geq \frac{1}{2}|\Delta|$.

Proof. Both L and l are nonincreasing functions of γ on $[0, \frac{1}{2}|\Delta|)$, while L is strictly increasing to $+\infty$ and l is strictly decreasing to $-\infty$ on $(\frac{1}{2}|\Delta|, \infty)$. From these observations we derive the graphs shown in figs. 1a–1c from which the assertions of the proposition can be read off. □

Remarks

(1) We will later show that the origin is the only stable solution for γ satisfying $\gamma \in (1/\kappa, k)$.

(2) In ref. [7], a result is proven which shows this stabilization for another general class of coupled oscillators.

3. Oscillators with no shear

In this section we assume that $q_1 = q_2 = 0$ and obtain quite explicit information about the evolution of solutions to (1.2) as the parameters $\Delta = \omega_2 - \omega_1$ and γ are varied. In section 3.1 we consider symmetric solutions to (1.2), i.e., solutions with $r_1 = r_2$. We show that, as the coupling strength γ increases from zero, the system passes through phase drift to locking. Depending on the frequency difference Δ, it may also pass through a region in which the rest state (with zero amplitude) is the only stable solution. The amplitudes are calculated explicitly, and a formula is given for the invariant torus which contains these solutions. Section 3.2 constructs nonsymmetric phase-locked solutions (i.e., $r_1 \neq r_2$) and shows that the symmetric solutions are the only stable phase locked solutions. Our main results in this section are summarized in figs. 4 and 5.

3.1. Symmetric solutions

We now turn to the full nonlinear behavior of (1.2), which is most transparant when there is no "shear," i.e., $q_1 = q_2 = 0$. (1.2) then becomes

$$\begin{aligned} \dot{r}_1 &= r_1\left(1 - \kappa\gamma - r_1^2\right) + \gamma r_2 \cos\phi, \\ \dot{r}_2 &= r_2\left(1 - \kappa\gamma - r_2^2\right) + \gamma r_1 \cos\phi, \\ \dot{\phi} &= \Delta - \gamma\left(r_2/r_1 + r_1/r_2\right)\sin\phi. \end{aligned} \tag{3.1}$$

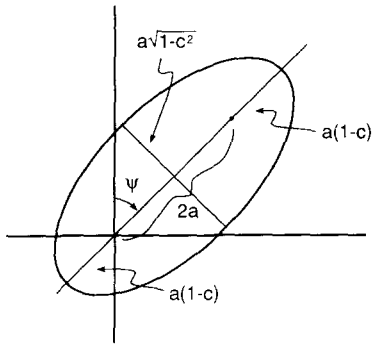

Fig. 2. The graph of (3.3) in the ρ^2, ϕ plane is an ellipse with major axis having an angle $\pi/2 - \psi$ from the horizontal axis.

We note that this system is symmetric with respect to r_1 and r_2; thus, we can look for solutions with $r_1 = r_2 = \rho$, which satisfy

$$\dot{\rho} = \rho(1 - \kappa\gamma - \rho^2) + \gamma\rho\cos\phi,$$
$$\dot{\phi} = \Delta - 2\gamma\sin\phi. \tag{3.2}$$

Clearly, solutions (ρ, ϕ) to (3.2) generate solutions (ρ, ρ, ϕ) to (3.1). The analysis of the transitions encountered in (3.2) as γ increases from 0 (no coupling) is made clearer by the observation that for a large range of parameters there is an invariant oval for (3.2). (This corresponds to an invariant torus in r_i, θ_i space.) To see this, we use the fact that (3.2) is equivalent under a change of variables to eq. (31) in ref. [1], for which an explicit solution was given in ref. [1]. Thus we have an explicit solution for (3.2). First, one solves the second equation of (3.2) for $\phi(t)$ by quadrature; then $\rho(t)$ is given by

$$\rho^2(t) = a(1 - c^2)/\{1 + c\sin[\varphi(t) + \psi]\}, \tag{3.3}$$

where $a = 1 - \kappa\gamma$, $c = \gamma/\sqrt{a^2 + \frac{1}{4}\Delta^2}$, and $\tan\psi = 2a/\Delta$. For $a > 0$ and $c \in [0, 1)$, i.e., for γ small enough, (3.3) describes a fourth-order oval. In (ρ^2, φ) coordinates (3.3) describes an ellipse whose major axis lies on the ray $\varphi = \pi/2 - \psi$ and whose foci are at the origin and at $(\rho^2, \varphi) = (2ac, \pi/2 - \psi)$. The major semi-axis of this ellipse has length a and its minor semi-axis has length $a\sqrt{1 - c^2}$ (fig. 2). For convenience, we shall use the ellipse interpretation. In ref. [1] it is shown that (3.3) is an asymptotically stable solution to (3.2) which attracts everything except the origin in $\mathbb{R}^2$. The ellipse persists as long as $c < 1$ and $a < 1$. The inequality $c < 1$ is equivalent to $(1 - \kappa^2)\gamma^2 + 2\kappa\gamma - (1 + \frac{1}{4}\Delta^2) < 0$, that is, $\gamma < k(\kappa, \Delta)$, while $a > 0$ is equivalent to $\gamma < 1/\kappa$ (cf. proposition 2.1).

The flow described by (3.2) contains no rest points if $2\gamma/|\Delta| < 1$. Thus, for γ small (3.2) describes the projection of a torus flow onto the (ρ, ϕ) space, i.e., a phase-drift solution. The behavior of (3.2) is best described by considering the two separate cases $|\Delta| > 2/\kappa$ and $|\Delta| < 2/\kappa$. Since the qualitative behavior is independent of the specific value of κ as long as $\kappa > 0$, we shall simplify the calculations by taking $\kappa = 1$. The behavior for $\kappa = 0$ is covered by the case $|\Delta| < 2/\kappa$.

(i) If $|\Delta| < 2$ then $\frac{1}{2}|\Delta| < k(1, \Delta) < 1$. For $\gamma \in (0, \frac{1}{2}|\Delta|)$ we have the torus flow (phase drift) described above and shown in fig. 3a. At $\gamma = \frac{1}{2}|\Delta|$ a saddle–node rest point appears and the ellipse becomes a homoclinic orbit (fig. 3b). This marks the onset of phase locking and the loss of drift. For $\gamma \in (\frac{1}{2}|\Delta|, k)$ the saddle–node splits into a saddle and a node, and the ellipse consists of a pair of heteroclinic orbits joining

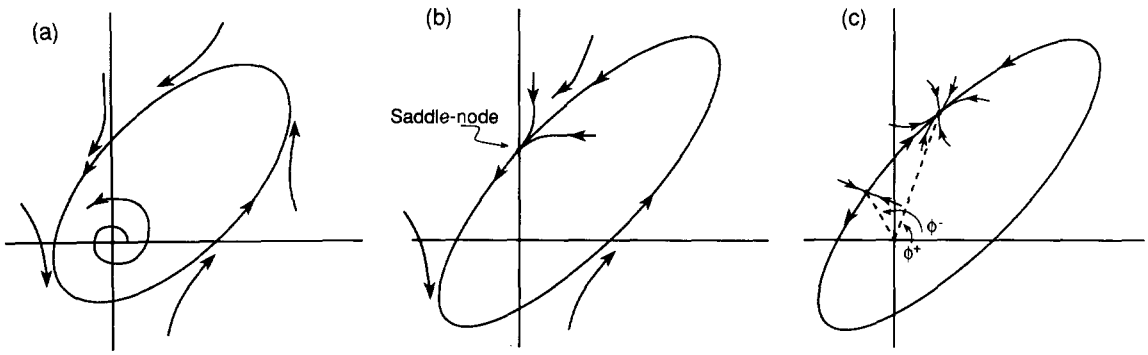

Fig. 3. Symmetric flow in the ρ^2, ϕ plane for $\Delta > 0$ and various values of γ. (a) $0 < \gamma < \frac{1}{2}\Delta$: stable phase drift; (b) $\gamma = \frac{1}{2}\Delta$: saddle–node bifurcation; (c) $\frac{1}{2}\Delta < \gamma < k$: saddle and sink joined by heteroclinic orbits. For $\gamma = k$, the saddle merges with the origin in a Hopf bifurcation, leaving only the sink, which persists $\forall\, \gamma \leq k$. For $\Delta < 0$, all the above flows have reversed orientation.

them (fig. 3c). The rest points are given by

$$\rho^2_{\pm} = 1 - \gamma \pm \sqrt{\gamma^2 - \tfrac{1}{4}\Delta^2}\,,$$
$$\phi_+ = \arcsin(\Delta/2\gamma), \qquad \phi_- = \pi - \arcsin(\Delta/2\gamma) \tag{3.4}$$

and represent a pair of phase-locked orbits. The "+" sign in (3.4) corresponds to the node and the "−" sign to the saddle. As $\gamma \uparrow k$, $c \uparrow 1$ and the ellipse gets thinner. At $\gamma = k$ the saddle merges with the origin and only the node remains. This coincides with the bifurcation at the origin described in proposition 2.1 and shows that it is a Hopf bifurcation. The node persists for all $\gamma > k$.

(ii) If $|\Delta| > 2$ then $1 < \frac{1}{2}|\Delta| < k(1, \Delta)$. For $\gamma \in (0, 1)$ we have the phase-drift torus flow shown in fig. 3a. However, as $\gamma \uparrow 1$, $\rho^2(\cdot) \to 0$ and the torus merges with the origin (Hopf bifurcation) at $\gamma = 1$ (cf. proposition 2.1). For $\gamma \in (1, k)$ there is no invariant ellipse and no nontrivial rest points for (3.2). As shown in section 2, for $\gamma \in (1, k)$ the origin is stable so that this is the parameter region associated with the Bar-Eli effect. For $\gamma = k$ there is a bifurcation in which the origin loses stability and, as can be seen from (3.4), the rest state (phase-locked orbit in r_i, θ_i space) $\rho = \rho_+, \phi = \phi_+$ emerges. This phase-locked orbit persists for all $\gamma > k$.

We now turn to the stability of the symmetric solutions constructed above, which must be investigated in the context of (3.1), not (3.2). To establish the stability of the phase-drift solutions, we rewrite (3.1) in coordinates adapted to the existence of a symmetric solution:

$$\sigma = \tfrac{1}{2}(r_1 - r_2), \qquad \tau = \tfrac{1}{2}(r_1 + r_2).$$

The resulting systems is

$$\dot{\sigma} = \sigma\left(a - \gamma\cos\phi - 3\tau^2 - \sigma^2\right),$$
$$\dot{\tau} = \tau\left(a + \gamma\cos\phi - \tau^2 - 3\sigma^2\right),$$
$$\dot{\phi} = \Delta - \frac{2\gamma(\tau^2 + \sigma^2)}{\tau^2 - \sigma^2}\sin\phi. \tag{3.5}$$

In these coordinates, the drift solution (which corresponds to an invariant torus in r_i, θ_i space) is given by

$\sigma = 0$, $\tau = \rho(t)$, $\phi = \phi(t)$, where ρ is defined by eq. (3.3) and $\phi(t)$ is any solution to $\phi' = \Delta - 2\gamma \sin\phi$. The variational system of (3.5) with respect to one of these periodic solutions is

$$V' = \begin{pmatrix} a - \gamma\cos\phi - 3\rho^2 & 0 & 0 \\ 0 & a + \gamma\cos\phi - 3\rho^2 & -\gamma\rho\sin\phi \\ 0 & 0 & -2\gamma\cos\phi \end{pmatrix} V. \tag{3.6}$$

The coefficient matrix in (3.6) is block diagonal and upper triangular. The Floquet multiplier associated with the upper 1×1 block is

$$\mu_1 = \exp\left(\int_0^T \left[a - \gamma\cos\phi(t) - 3\rho^2(t) \right] \mathrm{d}t \right),$$

while the multipliers associated with the lower 2×2 block are

$$\mu_2 = \exp\left(\int_0^T \left[a + \gamma\cos\phi(t) - 3\rho^2(t) \right] \mathrm{d}t \right)$$

and

$$\mu_3 = \exp\left(-2\gamma \int_0^T \cos\phi(t)\, \mathrm{d}t \right).$$

Since $\dot{\phi} = \Delta - 2\gamma\sin\phi \neq 0$ it is easy to check that

$$\int_0^T \cos\phi(t)\, \mathrm{d}t = 0.$$

Thus $\mu_3 = 1$ and the two multipliers corresponding to directions normal to the symmetric drift solution are equal: $\mu_1 = \mu_2 \equiv \mathrm{e}^I$, where

$$I \equiv \int_0^T \left[a - 3\rho^2(t) \right] \mathrm{d}t.$$

An integral similar to I was evaluated explicitly in ref. [1], and after a suitable transformation that result can be used to show that

$$I = -4\pi a \sqrt{\Delta^2 - 4\gamma^2}\,.$$

Since $\Delta^2 > 4\gamma^2$ for a drift solution, I is real and negative. Thus, as long as $\gamma < \min(1/\kappa, \frac{1}{2}|\Delta|)$, the phase-drift solution exists and it is stable, since $\mathrm{e}^I < 1$.

To check the stability of the critical points, we use (3.6) along with the formulas (3.4) for the rest points. Let $b = \sqrt{\gamma^2 - \frac{1}{4}\Delta^2}$, where b is real for $2\gamma/|\Delta| > 1$. The eigenvalues for the positive branch are $-2b$, $-2(a+b)$, $-2(a+2b)$, so that this branch is always stable. The eigenvalues for the negative branch are $2b$, $2(b-a)$, $2(2b-a)$. Since $b > 0$, this branch is always unstable. There are bifurcations at $a = 2b$ and $a = b$. Since $a = b$ if and only if $\gamma = k$, this bifurcation corresponds to the disappearance of the negative branch when it hits the origin. The bifurcation at $a = 2b$ corresponds to the interaction of the negative

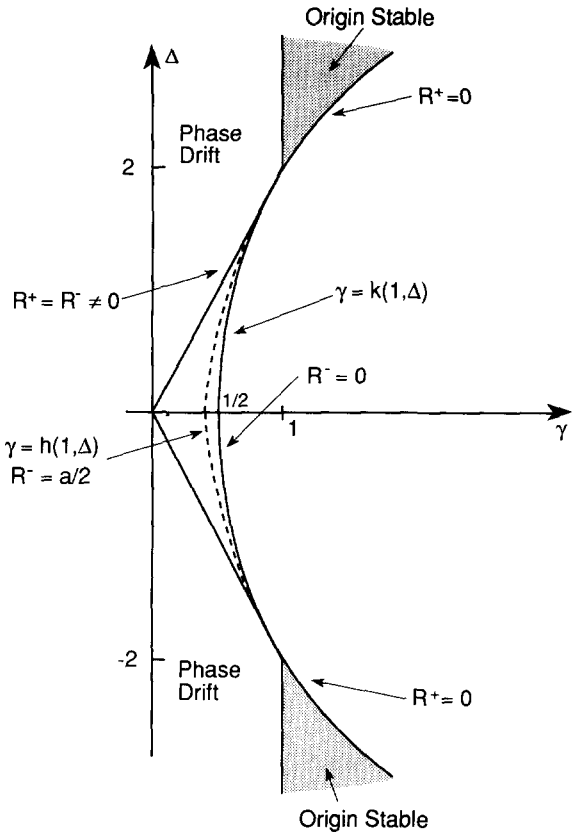

Fig. 4. The bifurcation curves in the γ, Δ parameter planes for the symmetric ρ, ϕ flow.

branch with the symmetric solutions (see section 3.2) and occurs when γ satisfies

$$3\gamma^2 + 2\gamma - (1 + \Delta^2) = 0, \tag{3.7}$$

i.e., when $\gamma = h(1, \Delta) \equiv \frac{1}{3}(\sqrt{4 + 3\Delta^2} - 1)$.

The bifurcation curves in the (γ, Δ) parameter plane for the symmetric solutions are shown in fig. 4. The phase-drift solution is the only symmetric solution in the set $\{(\gamma, \Delta) \in \mathbb{R}^2: 0 < \gamma < \min(\frac{1}{2}|\Delta|, 1)\}$ and it is stable. For $|\Delta| \in (0, 2)$, phase drift ends with the emergence of two symmetric phase-locked solutions (one stable and one unstable) on the line $\gamma = \frac{1}{2}|\Delta|$. These persist for $\gamma \in (\frac{1}{2}|\Delta|, k(1, \Delta))$ with the unstable one disappearing at the origin in a Hopf bifurcation on the curve $\gamma = k(1, \Delta)$. For $\gamma > k(1, \Delta)$ there is a unique symmetric phase-locked solution and it is stable. For $|\Delta| \in (2, \infty)$ the phase drift ends with a Hopf bifurcation at the origin on the line $\gamma = 1$. For $\gamma \in (1, k(1, \Delta))$ we are in the Bar-Eli region where only the rest state at the origin is stable. This ends on the curve $\gamma = k(1, \Delta)$ with a Hopf bifurcation in which the origin looses stability and a stable phase-locked solution emerges. The stable phase-locked solution persists for all $\gamma > k(1, \Delta)$. In figs. 5a–5c, we give the corresponding bifurcation diagrams in the $(\gamma, \max r_1)$ plane for $|\Delta| \in (0, 2)$, $|\Delta| = 2$ and $|\Delta| \in (2, \infty)$. These diagrams also show two branches of asymmetric phase-locked solutions, which we will discuss more fully in subsection 3.2. The asymmetric solutions intersect the unstable phase-locked branch along the curve $\gamma = h(1, \Delta)$ given by (3.7) and shown in fig. 4. Note that $\frac{1}{2}|\Delta| < h(1, \Delta) < k(1, \Delta)$ for $|\Delta| \in [0, 2)$ and that the curves $\gamma = \frac{1}{2}|\Delta|$, $\gamma = h(1, \Delta)$ and $\gamma = k(1, \Delta)$ are all tangent to one another at $|\Delta| = 2$.

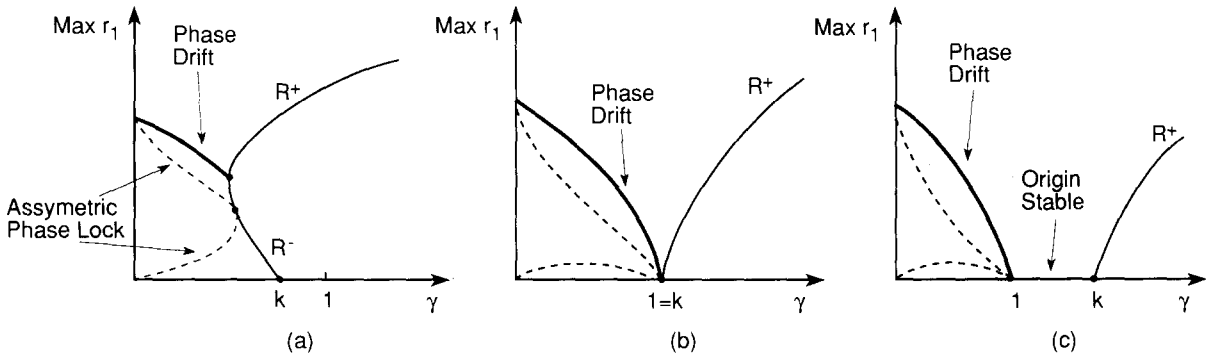

Fig. 5. The bifurcation diagram in the γ, max r_1 plane for various fixed values of Δ. The flow is the same as in fig. 4. (a) $|\Delta| \in (0,2)$: phase-locked solution emerges from finite amplitude phase drift by the mechanism shown in figs. 3a–3c. (b) $|\Delta| = 2$: transitional case. (c) $|\Delta| \in (2,\infty)$: as γ increases, the phase-drift solution collapses in a Hopf bifurcation that leaves the origin stable. For $\gamma > k$, there is a stable phase lock.

3.2. *Asymmetric solutions*

We now consider the asymmetric phase-locked solutions of (3.1), i.e., solutions in which $r_1 \neq r_2$. Indeed, we shall construct all the equilibrium solutions to (3.1). The equilibria satisfy

$$r_1(a - r_1^2) = -\gamma r_2 \cos\phi, \qquad r_2(a - r_2^2) = -\gamma r_1 \cos\phi,$$
$$\Delta = \gamma(r_2/r_1 + r_1/r_2)\sin\phi. \tag{3.8}$$

Again, we shall assume that $\kappa = 1$, so $a = 1 - \gamma$. We take the ratio of the first two equations and obtain

$$r_1^2(a - r_1^2) = r_2^2(a - r_2^2).$$

Thus, either $r_1^2 = r_2^2$ or $r_1^2 = (a - r_2^2)$. The former are just the symmetric solutions that we have already considered. As we have done in section 3.1, we can reduce (3.8) to a single equation for r_1^2:

$$r_1^2 = \tfrac{1}{2}a\left[1 \pm \sqrt{1 - 4\gamma^2/(a^2 + \Delta^2)}\right]. \tag{3.9}$$

Asymmetric solutions exist if and only if $a > 0$ and $1 - 4\gamma^2/(a^2 + \Delta^2) \geq 0$. Therefore, for $|\Delta| < 2$, γ must lie between 0 and the hyperbola described by (3.7) (cf. fig. 4). At $\gamma = h(1, \Delta)$ there is a turning point bifurcation and both asymmetric branches terminate on the unstable symmetric phase-locked branch with $r_1^2 = r_2^2 = \frac{1}{2}a$ (cf. fig. 5). For $|\Delta| > 2$, the asymmetric solutions exist only if $0 < \gamma < 1$. In that case, they end in a Hopf bifurcation at the origin, with $\gamma = 1$ (cf. figs. 5b and 5c). We prove below that these solutions are always asymptotically unstable.

The Jacobian for (3.1) is

$$\begin{pmatrix} 1 - \kappa\gamma - 3r_1^2 & \gamma\cos\phi & -r_2\gamma\sin\phi \\ \gamma\cos\phi & 1 - \kappa\gamma - 3r_2^2 & -r_1\gamma\sin\phi \\ -\gamma\sin\phi\,(1/r_2 - r_2/r_1^2) & -\gamma\sin\phi\,(1/r_1 - r_1/r_2^2) & -\gamma\cos\phi\,(r_2^2 + r_1^2)/r_1 r_2 \end{pmatrix}. \tag{3.10}$$

Multiplying the first and second equations of (3.8) by r_2 and r_1 respectively and adding, we see that

$$-\gamma \cos\phi \left(\frac{r_2^2 + r_1^2}{r_1 r_2} \right) = a.$$

Thus, the trace of (3.10) is identically 0. A very tedious calculation shows that the determinant of (3.10), evaluated at the asymmetric critical points, is $-2a(a^2 + \Delta^2 - 4\gamma^2)$, so the determinant is negative when a is positive. We conclude that for $a > 0$ and $\gamma < h(1, \Delta)$, two eigenvalues of (3.10) have positive real part and one has negative real part; thus the solutions are unstable.

Remark. We recall that there is an invariant ellipse for (3.2) as long as $\gamma < k$. For $|\Delta| < 2$, the unstable asymmetric branch of phase-locked solutions coincides with the unstable branch of symmetric ones when (3.7) is satisfied. This happens for a value of γ that is less than k. Thus, at that point, the invariant ellipse does not vanish, but it changes its stability type.

4. Symmetrically coupled oscillators: nonzero shear

In this section we discuss the behavior of a system of coupled oscillators with nonzero shear. Specifically, we assume that $q_j \neq 0$ for $j = 1$ and 2 so that each oscillator has a local frequency that depends on amplitude. The new phenomena we shall find occur for $\nu \equiv q_1 - q_2 > 0$. As we observed in section 2.1, shear does not affect the stability or instability of the zero rest state so that, in particular, we still have the Bar-Eli effect occurring in the same subset of the parameter space. However, for nonzero shear the transition from phase drift to phase lock is much more complicated than in the zero shear case. As we shall show, there is a region in the (γ, Δ) parameter half-plane where the transition occurs in the manner described in section 2, i.e., the saddle–nodes which occur at the onset of phase lock break the phase-drift solution. However, for $\nu > 0$ there are also parameter regions in which the system is *bistable*, with phase lock coexisting with either stable phase drift or stable rest at zero. Although in the nonzero shear case we do not have an explicit representation of the phase-drift solution, we are still able to prove these assertions. We will, however, rely on numerical evidence for some of the details, particularly for the global bifurcations that shape the bistable regimes.

Our analysis is elementary but rather complicated, so we begin with a brief outline. In section 4.1 we consider the symmetric phase-locked solutions and, in particular, find the bifurcation curves in the parameter plane along which these solutions are born or die. Changes in stability on these curves provide important clues to the global bifurcation picture, and some of these changes occur when symmetric solutions interact with asymmetric ones. In section 4.2 we find the curve along which symmetric and asymmetric branches of solutions intersect. In section 4.3 we do the stability calculations for the symmetric phase locked solutions along the curves identified in sections 4.1 and 4.2. These results are summarized in fig. 6 (which should be contrasted with fig. 4) and in proposition 4.1.

In section 4.4 we investigate the existence, uniqueness and stability of symmetric phase drift solutions. We combine some standard theory of codimension-two bifurcations with detailed phase plane analysis to show the existence of regions in parameter space where the system is bistable with a stable locked solution coexisting with either a stable phase drift solution or stable rest at zero. In addition, we use the results of our numerical studies to provide a detailed description of various transition mechanisms, particularly those

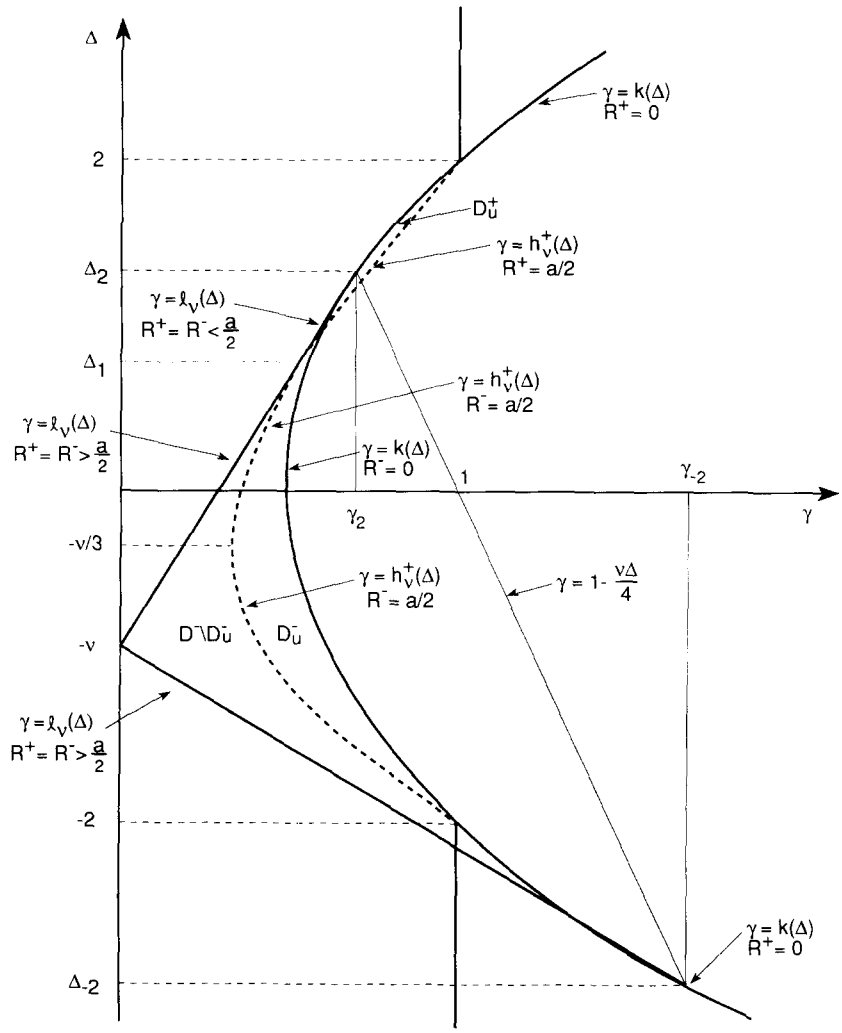

Fig. 6. Bifurcation diagram in γ, Δ parameter plane for the symmetric ρ, ϕ flow in the presence of shear. Note that the symmetries in fig. 2 have been broken.

by which bistability is lost. The subsection ends with some rather complicated bifurcation diagrams which represent our proposed synthesis of all the analytical and numerical evidence (figs. 15, 16 and 18).

In the final subsection, 4.5, we describe the effect of shear on the frequency of the phase-locked system. These effects are qualitatively as well as quantitatively dependent on the nature of the coupling, i.e., on the value of κ.

In the zero shear case, for γ sufficiently small, the only stable solution is phase drift. As γ is increased, stable phase lock results either from an infinite period bifurcation on the phase drift solution for $|\Delta| < 2$ or, for $|\Delta| > 2$, as a bifurcation from the stable rest state at zero after the phase drift solution has disappeared (Bar-Eli effect). The curves along which these bifurcations occur, together with the curves along which the symmetric and asymmetric phase-locked solution intersect, are all tangent at the degenerate bifurcation points $(1, \pm 2)$ in fig. 4. For $\nu > 0$ these degenerate points are partially unfolded and

the corresponding bifurcation curves do not have a common intersection (cf. fig. 6). As we shall see, this is the source of new phenomena in the nonzero shear case.

4.1. Symmetric phase-locked solutions

To find symmetric solutions to (1.2) set $\rho = r_1 = r_2$. The system reduces to

$$\dot{\rho} = \rho(a - \rho^2 + \gamma\cos\phi), \qquad \dot{\phi} = \Delta + \nu\rho^2 - 2\gamma\sin\phi. \tag{4.1}$$

Symmetric phase-locked solutions to (1.2) are obtained by solving the equations

$$a - R + \gamma\cos\phi = 0, \qquad \sin\phi = (\Delta + \nu R)/2\gamma, \tag{4.2}$$

where $R = \rho^2$. If $\nu = 0$ these equations are the same as the corresponding equations in the no-shear case, so we assume without loss of generality that $\nu > 0$. The solutions to (4.2) are given by

$$R^{\pm} = (1/s)\left[4a - \nu\Delta \pm \sqrt{(4a - \nu\Delta)^2 - s(4a^2 - 4\gamma^2 + \Delta^2)}\right], \tag{4.3}$$
$$\sin\phi^{\pm} = (\Delta + \nu R^{\pm})/2\gamma, \qquad \cos\phi^{\pm} = (R^{\pm} - a)/\gamma,$$

where $s = 4 + \nu^2$. (For $\nu = 0$, (4.3) reduces to (3.4).) It is clear that $\partial R^-/\partial\gamma < 0$, and it can be shown that $\partial R^+/\partial\gamma > 0$ whenever they are defined.

Nonzero symmetric phase-locked solutions are born in a saddle–node bifurcation and satisfy

$$R^+ = R^- = (4a - \nu\Delta)/s > 0. \tag{4.4}$$

In view of (4.3), they are characterized by

$$(4a - \nu\Delta)^2 = s(4a^2 - 4\gamma^2 + \Delta^2).$$

We solve for γ, with the simplifying assumption $\kappa = 1$ (so $a = 1 - \gamma$), to obtain

$$\gamma = \tfrac{1}{4}\left[-\nu(\Delta + \nu) \pm \sqrt{s}\,|\Delta + \nu|\right].$$

Choosing the sign so that $\gamma \geq 0$, this becomes

$$\begin{aligned} \gamma = l_\nu(\Delta) &\equiv \tfrac{1}{4}(\Delta + \nu)(\sqrt{s} - \nu) \equiv l_\nu^+(\Delta) \qquad \text{if } \Delta + \nu \geq 0, \\ &\equiv -\tfrac{1}{4}(\Delta + \nu)(\sqrt{s} + \nu) \equiv l_\nu^-(\Delta) \quad \text{if } \Delta + \nu < 0. \end{aligned} \tag{4.5}$$

The condition $R^{\pm} > 0$ means that we want only that part of the curve (4.5) which lies to the left of the line:

$$\gamma = 1 - \tfrac{1}{4}\nu\Delta.$$

This line intersects $\gamma = l(\Delta)$ at the points $P_{\pm 2} = (\gamma_{\pm 2}, \Delta_{\pm 2})$, where

$$\Delta_2 = \sqrt{s} - \nu, \qquad \Delta_{-2} = -(\sqrt{s} + \nu), \qquad \gamma_2 = \tfrac{1}{4}\sqrt{s}\,\Delta_2, \qquad \gamma_{-2} = -\tfrac{1}{4}\sqrt{s}\,\Delta_{-2}.$$

Note that $\Delta_2 \in (0, 2)$ and $\Delta_{-2} \in (-\infty, -2)$ (fig. 6).

On the curve (4.5), $R^{\pm} = R^{\pm}(l(\Delta), \Delta)$ decreases from 1 at $(0, -\nu)$ to 0 at $P_{\pm 2}$. In view of (4.3), (4.4) and (4.5)

$$\cos\phi^{\pm}(l(\Delta), \Delta) = -\nu/\sqrt{s} \quad \text{if } \Delta + \nu \geq 0,$$
$$= \nu/\sqrt{s} \quad \text{if } \Delta + \nu < 0$$

and

$$\sin\phi^{\pm}(l(\Delta), \Delta) = 2/\sqrt{s} \quad \text{for } \Delta \in (\Delta_{-2}, \Delta_2).$$

For $\Delta \in (\Delta_{-2}, \Delta_2)$, the R^+ branch of phase-locked solutions persists (i.e., $R^+ > 0$) everywhere to the right of $\gamma = l(\Delta)$. The R^- branch disappears (i.e., $R^- = 0$) in a bifurcation at the origin along the parabola

$$\gamma = k(\Delta) \equiv \tfrac{1}{2}(1 + \tfrac{1}{4}\Delta^2).$$

(In section 3 we used the notation $\gamma = k(1, \Delta)$ for this parabola.) Note that the curve $\gamma = k(\Delta)$ is tangent to $\gamma = l_\nu(\Delta)$ at the points P_{-2} and P_2 (cf. fig. 6). For $\Delta \in (-\infty, \Delta_{-2}) \cup (\Delta_2, \infty)$ the R^- branch of (4.3) does not exist and the only symmetric phase-locked solutions are on the R^+ branch. In this case the R^+ branch bifurcates from zero along the parabola $\gamma = k(\Delta)$ and persists everywhere to the right of it. We define the C^1 function

$$p_\nu(\Delta) \equiv l_\nu(\Delta) \quad \text{on } [\Delta_{-2}, \Delta_2]$$
$$\equiv k(\Delta) \quad \text{on } \mathbb{R} \setminus [\Delta_{-2}, \Delta_2]. \tag{4.6}$$

The R^+ branch of phase-locked solutions is born on the curve $\gamma = p_\nu(\Delta)$ in a saddle–node bifurcation with the R^- branch for $\Delta \in [\Delta_{-2}, \Delta_2]$ and, as we shall show in section 4.4, in a saddle–node bifurcation at zero for $\Delta \notin [\Delta_{-2}, \Delta_2]$.

4.2. *Asymmetric phase-locked solutions*

Asymmetric phase-locked solutions of (1.2) are found by solving the equations

$$r_1^2 + r_2^2 = a,$$
$$r_1\sqrt{a - r_1^2} + \gamma\cos\phi = 0,$$
$$\Delta - aq_2 + (q_1 + q_2)r_1^2 - \frac{\gamma a}{r_1\sqrt{a - r_1^2}}\sin\phi = 0, \tag{4.7}$$

where we are again assuming that $\kappa = 1$ so that $a = 1 - \gamma$. There is nothing to be gained by attempting to actually solve these equations since we shall be interested only in the intersections of the symmetric and asymmetric branches of solutions. In view of (4.7), asymmetric solutions can exist only for $a > 0$, i.e., for $\gamma \in [0, 1)$. Moreover, it follows from (4.7) that intersections of symmetric and asymmetric branches are characterized by $r_1^2 = r_2^2 = \frac{1}{2}a$. Thus, by (4.3), they occur when

$$(16 - s)\gamma^2 + 2(s + 2\nu\Delta)\gamma - s - 4\nu\Delta - 4\Delta^2 = 0.$$

Naturally, this equation reduces to (3.7) for $\nu = 0$. Solving for γ we find that $R^{\pm} = \frac{1}{2}a$ on the curves

$$\begin{aligned} \gamma &= h_\nu^+(\Delta) \quad \text{for } \Delta \in [-2,2] \quad \text{if } 0 \le \nu \le 4, \\ &= h_\nu^+(\Delta) \quad \text{for } \Delta \in [\tilde{\Delta},2] \quad \text{if } \nu > 4, \\ &= h_\nu^-(\Delta) \quad \text{for } \Delta \in (\tilde{\Delta},-2] \quad \text{if } \nu > 4, \end{aligned} \tag{4.8}$$

where

$$h_\nu^{\pm}(\Delta) \equiv \frac{1}{12-\nu^2}\left(-s - 2\nu\Delta \pm 4\sqrt{3\Delta^2 + 4\nu\Delta + s}\right) \quad \text{for } \nu \neq 2\sqrt{3},$$

$$h_{2\sqrt{3}}^+(\Delta) = (\Delta^2 + 2\sqrt{3}\Delta + 4)/(2\sqrt{3}\Delta + 8),$$

and

$$\tilde{\Delta} = \tfrac{1}{3}(\sqrt{\nu^2 - 12} - 2\nu).$$

The curves $\gamma = h_\nu^{\pm}(\Delta)$ are hyperbolic and $h_0^+(\Delta)$ coincides with $h(1,\Delta)$ defined below (3.7). The restriction in (4.8) to segments of these hyperbolae ensures that $\gamma \le 1$, i.e. $a \ge 0$. Note that $h_\nu^+(-\frac{1}{3}\nu) = \frac{1}{3}$ and $\mathrm{d}h_\nu^+(-\frac{1}{3}\nu)/\mathrm{d}\Delta = 0$, while $h_\nu^+(\tilde{\Delta}) = h_\nu^-(\tilde{\Delta})$ and $\mathrm{d}h_\nu^{\pm}(\tilde{\Delta})/\mathrm{d}\Delta = \mp\infty$ for $\nu > 2\sqrt{3}$. Moreover $h_\nu^+(\pm 2) = 1$ if $0 \le \nu \le 4$ and $h_\nu^{\pm}(\pm 2) = 1$ if $\nu > 4$. In all cases the curves (4.8) lie in the strip $\frac{1}{3} \le \gamma \le 1$ and terminate at the points $(1, \pm 2)$ (cf. fig. 6). To avoid an unprofitable proliferation of cases *we will assume from now on that* $0 \le \nu < 4$.

In view of (4.4), the condition that the saddle–nodes born on $\gamma = l_\nu(\Delta)$ satisfy $R^{\pm} = \frac{1}{2}a$ is

$$(4-\nu^2)[1 - l_\nu(\Delta)] = 2\nu\Delta. \tag{4.9}$$

Solving (4.9) on the lower branch $l = l_\nu^-$ of (4.5) we obtain $\Delta = (\nu^2 - 4)/(\sqrt{s} - 2\nu)$. From (4.5) the corresponding value of γ is

$$\gamma = \sqrt{s}/(\sqrt{s} - 2\nu).$$

Thus either $\gamma < 0$ or $\gamma > 1$ and it follows that $R^{\pm} = \frac{1}{2}a > 0$ *cannot hold on* $\gamma = l_\nu^-(\Delta)$. The solution to (4.9) for $l = l_\nu^+$ is

$$\Delta_1 \equiv (4-\nu^2)/(\sqrt{s} + 2\nu)$$

and

$$\gamma_1 = l_\nu^+(\Delta_1) = \sqrt{s}/(\sqrt{s} + 2\nu).$$

One can verify that $\gamma_1 \in (\frac{1}{3}, \gamma_2)$, $\Delta_1 \in (-\frac{1}{3}\nu, \Delta_2)$ and $\gamma_1 = h_\nu^+(\Delta_1)$. Indeed, $\gamma = h_\nu^+(\Delta)$ *is tangent to* $\gamma = l_\nu^+(\Delta)$ at $P_1 \equiv (\gamma_1, \Delta_1)$ (cf. fig. 6). As we shall see in section 4.3, P_1 is a degenerate bifurcation point which plays an important role in the analysis of the coexistence of phase-drift and phase-locked solutions (see section 4.4).

Since $R^{\pm} > \frac{1}{2}a$ on (4.5) for $\Delta \in [-2, \Delta_1)$ and R^- decreases with increasing γ for fixed Δ, it is possible that the R^- branch intersects the asymmetric solutions (with $R^- = \frac{1}{2}a$) on $\gamma = h_\nu^+(\Delta)$. On the other hand,

$R^{\pm} < \frac{1}{2}a$ on (4.5) for $\Delta \in (\Delta_1, \Delta_2)$ and $R^{\pm} = 0 < \frac{1}{2}a$ on (4.6) for $\Delta \in [\Delta_2, 2)$. Since R^+ increases with increasing γ for fixed Δ, it is possible that the R^+ branch and the asymmetric solutions intersect on $\gamma = h_\nu^+(\Delta)$ for $\Delta \in (\Delta_1, 2)$. As we shall see from the stability analysis in section 4.3, all of these potential intersections actually do occur since $\gamma = h_\nu^+(\Delta)$ is a bifurcation curve for the R^- branch on $(-2, \Delta_1)$ and for the R^+ branch on $(\Delta_1, 2)$.

4.3. *Stability of symmetric phase-locked solutions*

As in section 3.1, to investigate stability of symmetric solutions we introduce the coordinates $\sigma \equiv \frac{1}{2}(r_1 - r_2)$ and $\tau = \frac{1}{2}(r_1 + r_2)$. In these coordinates (1.2) becomes

$$\begin{aligned}
\dot{\sigma} &= \sigma(a - \gamma\cos\phi - 3\tau^2 - \sigma^2), \\
\dot{\tau} &= \tau(a + \gamma\cos\phi - \tau^2 - 3\sigma^2), \\
\dot{\phi} &= \Delta + \nu(\sigma^2 + \tau^2) + 2\mu\sigma\tau - 2\gamma\left(\frac{\tau^2 + \sigma^2}{\tau^2 - \sigma^2}\right)\sin\phi,
\end{aligned} \tag{4.10}$$

where $\mu \equiv q_1 + q_2$. The symmetric phase-locked solutions are given by $\sigma = 0$, $\tau = \sqrt{R^{\pm}}$, $\sin\phi = (\Delta + \nu R^{\pm})/2\gamma$, and $\cos\phi = (R^{\pm} - a)/\gamma$. The differential of the right-hand side of (4.10) evaluated on a symmetric phase-locked solution, is

$$J = \begin{pmatrix} 2(a - 2R) & 0 & 0 \\ 0 & -2R & -\frac{1}{2}\sqrt{R}\,(\Delta + \nu R) \\ 2\mu\sqrt{R} & 2\nu\sqrt{R} & 2(a - R) \end{pmatrix}, \tag{4.11}$$

where $R = R^{\pm}$. The eigenvalues of J are

$$\begin{aligned}
\lambda_1(R) &= 2(a - 2R), \\
\lambda_j(R) &= a - 2R + (-1)^j\sqrt{(a - 2R)^2 - R[sR - (4a - \nu\Delta)]} \quad (j = 2, 3).
\end{aligned}$$

Since J is block triangular, λ_2 and λ_3 are the eigenvalues of the lower right-hand 2×2 block and govern stability in the plane $\sigma = 0$, while λ_1 is the eigenvalue of the upper left-hand 1×1 block and governs stability in the complimentary space $\sigma \neq 0$. Note that, as in section 3.1, $\lambda_1 = \lambda_2 + \lambda_3$; as we will see below, this forces a non-generic bifurcation.

To describe the evolution in parameter space of the stability of an equilibrium $(0, \sqrt{R}, \phi)$ it is convenient to use its *signature*

$$\mathcal{S}(R) \equiv (e_1, e_2, e_3),$$

where

$$\begin{aligned}
e_j &= + \quad \text{if } \mathrm{Re}\,\lambda_j(R) > 0, \\
&= 0 \quad \text{if } \mathrm{Re}\,\lambda_j(R) = 0, \\
&= - \quad \text{if } \mathrm{Re}\,\lambda_j(R) < 0 \quad (j = 1, 2, 3).
\end{aligned}$$

An equilibrium is asymptotically stable if and only if its signature is $(-,-,-)$. In stating the main result of this section we will use several subregions of the (γ, Δ) parameter space:

$$D^+ \equiv \{(\gamma,\Delta): \gamma > p_\nu(\Delta), \Delta \in \mathbb{R}\},$$
$$D_u^+ \equiv \{(\gamma,\Delta): p_\nu(\Delta) < \gamma < h_\nu(\Delta), \Delta_1 < \Delta < 2\},$$
$$D^- \equiv \{(\gamma,\Delta): l_\nu(\Delta) < \gamma < k(\Delta), \Delta_{-2} < \Delta < \Delta_2\},$$

and

$$D_u^- \equiv \{(\gamma,\Delta): h_\nu(\Delta) < \gamma < k(\Delta), -2 < \Delta < \Delta_1\} \cup \{(\gamma,\Delta): l_\nu(\Delta) < \gamma < k(\Delta), \Delta_1 \le \Delta < \Delta_2\}.$$

These subregions are shown in fig. 6.

Proposition 4.1.

(a) The R^+ branch of phase-locked solutions exists in the region D^+ and has signature

$$\mathcal{S}(R^+) = (+,+,+) \quad \text{in } D_u^+$$
$$= (-,-,-) \quad \text{in the interior of } D^+ \setminus D_u^+.$$

(b) The R^- branch of phase-locked solutions exists in the region D^- and has signature

$$\mathcal{S}(R^-) = (+,+,-) \quad \text{in } D_u^-$$
$$= (-,+,-) \quad \text{in the interior of } D^- \setminus D_u^-.$$

Recall that in section 2 we proved that the rest state at the origin is asymptotically stable for (1.2) in the parameter region $\{(\gamma,\Delta): 1 < \gamma < k(\Delta), |\Delta| > 2\}$. Combining this with proposition 4.1a we obtain

Corollary 4.2. The system (1.2) is bistable with both the rest state at the origin and the symmetric phase-locked state (ϕ^+, R^+) asymptotically stable in the parameter region

$$\{(\gamma,\Delta): \max(1, l_\nu(\Delta)) < \gamma < k(\Delta), \Delta_{-2} < \Delta < -2\}.$$

Proof of proposition 4.1a. Let

$$m \equiv \max(0, (4a - \nu\Delta)/s).$$

If $\Delta \in (-\infty, \Delta_1) \cup (2, \infty)$ then the R^+ branch of phase-locked solutions is born on $\gamma = p_\nu(\Delta)$ with $R^+ = m > \frac{1}{2}a$ so that $\mathcal{S}(R^+) = (-,0,-)$. In view of (4.3) and the results proved in section 4.2, $R^+ > \max(m, \frac{1}{2}a)$ for $\gamma > p_\nu(\Delta)$. Thus $a - 2R^+ < 0$ and $\operatorname{Re}\lambda_2(R^+) < a - 2R^+ + |a - 2R^+| = 0$. It follows that $\mathcal{S}(R^+) = (-,-,-)$ for $\gamma > p_\nu(\Delta)$ and $\Delta \notin [\Delta_1, 2]$.

For $\Delta \in (\Delta_1, 2)$ we have $R^+ = m < \frac{1}{2}a$ on $\gamma = p_\nu(\Delta)$ and hence $\mathcal{S}(R^+) = (+,+,0)$. If $p_\nu(\Delta) < \gamma < h_\nu(\Delta)$ then $m < R^+ < \frac{1}{2}a$. Therefore $\operatorname{Re}\lambda_2(R^+) > 0$ and it follows that $\mathcal{S}(R^+) = (+,+,+)$. For $\gamma = h_\nu(\Delta)$ we

have $m < R^+ = \frac{1}{2}a$. Consequently $\lambda_1(R^+) = 0$ and

$$\lambda_j(R^+) = (-1)^j \mathrm{i}\sqrt{R^+[(4a - \nu\Delta) - sR^+]} \quad (j = 2, 3)$$

so that $\mathscr{S}(R^+) = (0,0,0)$. Finally, if $\gamma > h_\nu(\Delta)$ then $R^+ > \max(m, \frac{1}{2}a)$ and $\mathscr{S}(R^+) = (-,-,-)$. □

Remark. Because of the relationship $\lambda_1 = \lambda_2 + \lambda_3$, the bifurcation which occurs on the R^+ branch as the parameter point crosses the curve $\gamma = h_\nu^+(\Delta)$ for $\Delta \in (\Delta_1, 2)$ combines a Hopf bifurcation in the $\sigma = 0$ plane (complex eigenvalues λ_2 and λ_3 cross the imaginary axis) and a transcritical bifurcation in the complementary space $\sigma \neq 0$ corresponding to an intersection of the R^+ branch with the asymmetric solutions. Although the combination of these bifurcations is nongeneric, the Hopf bifurcation in the plane $\sigma = 0$ is generic since it occurs on the Hopf curve which emanates from the degenerate saddle-node bifurcation at the Bogdanov-Takens point P_1 (cf. section 4.4).

Proof of proposition 4.1b. The R^+ and R^- branches of phase-locked solutions coincide on $\gamma = l_\nu(\Delta)$. Thus

$$\begin{aligned} \mathscr{S}(R^-) &= (-,0,-) \quad \text{for } \Delta \in (\Delta_{-2}, \Delta_1), \\ &= (+,+,0) \quad \text{for } \Delta \in (\Delta_1, \Delta_2). \end{aligned}$$

If $\Delta \in (\Delta_1, \Delta_2)$ then the R^- branch persists for $l_\nu(\Delta) < \gamma < k(\Delta)$ with

$$0 < R^- < \min\big((4a - \nu\Delta)/s, \tfrac{1}{2}a\big)$$

so that $\mathscr{S}(R^-) = (+,+,-)$. For $\gamma = k(\Delta)$ we have $R^- = 0$ and $\mathscr{S}(R^-) = (+,+,0)$. If $\Delta \in (\Delta_{-2}, -2)$ then the R^- branch persists for $l_\nu(\Delta) < \gamma < k(\Delta)$ with

$$\tfrac{1}{2}a < R^- < (4a - \nu\Delta)/s.$$

Therefore $\mathscr{S}(R^-) = (-,+,-)$. On $\gamma = k(\Delta)$, $\mathscr{S}(R^-) = (-,0,-)$. Finally, if $\Delta \in (-2, \Delta_1)$ then

$$\begin{aligned} &\tfrac{1}{2}a < R^- < (4a - \nu\Delta)/s && \text{if } l_\nu(\Delta) < \gamma < h_\nu(\Delta), \\ &R^- = \tfrac{1}{2}a && \text{if } \gamma = h_\nu(\Delta), \text{and} \\ &0 < R^- < \min\big((4a - \nu\Delta)/s, \tfrac{1}{2}a\big) && \text{if } h_\nu(\Delta) < \gamma < k(\Delta). \end{aligned}$$

It follows that

$$\begin{aligned} \mathscr{S}(R^-) &= (-,+,-) \quad \text{for } l_\nu(\Delta) < \gamma < h_\nu(\Delta), \\ &= (0,+,-) \quad \text{for } \gamma = h_\nu(\Delta), \\ &= (+,+,-) \quad \text{for } h_\nu(\Delta) < \gamma < k(\Delta), \\ &= (+,+,0) \quad \text{for } \gamma = k(\Delta). \end{aligned}$$

□

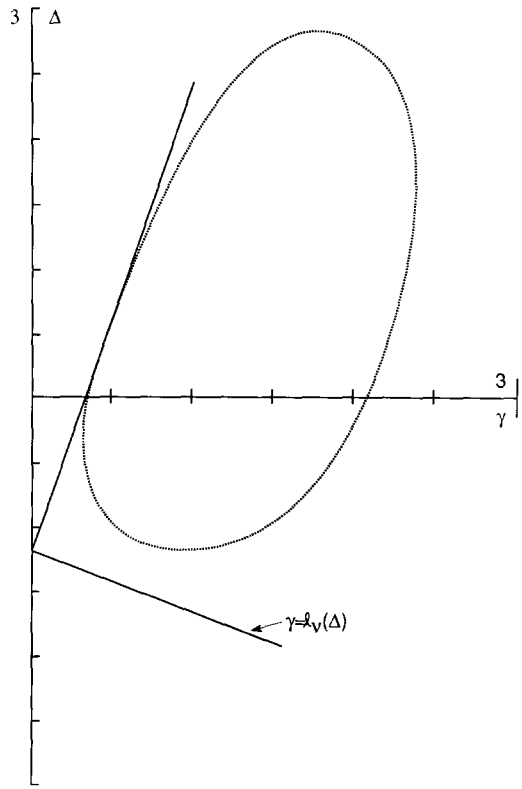

Fig. 7. A region in which $\lambda_2(R^+)$ and $\lambda_3(R^+)$ are complex for $\nu = 1.2$.

Remarks

(1) Proposition 4.1a and corollary 4.2 are independent of the value of $\nu > 0$. If $\nu > 4$ then proposition 4.1b holds if we add to D_u^- the region

$$\{(\gamma, \Delta): h_\nu^+(\Delta) < \gamma < h_\nu^-(\Delta), \tilde{\Delta} < \Delta \leq -2\}.$$

(2) For $\Delta \in (\Delta_1, 2)$, the eigenvalues $\lambda_2(R^+)$ and $\lambda_3(R^+)$ are pure imaginary on the curve $\gamma = h_\nu^+(\Delta)$ given by (4.8). Thus they are certainly complex for parameter points in some neighborhood of (4.8). Fig. 7 shows the parameter region where $\lambda_2(R^+)$ and $\lambda_3(R^+)$ are complex for a typical value of $\nu \in (0, 2)$. Observe that the boundary of this region is tangent to the line $\gamma = l_\nu^+(\Delta)$ at (γ_1, Δ_1). For $\nu = 0$, the $\lambda_j(R^+)$ are all real and the region of complexity shown in fig. 7 degenerates into the segment $\{(\gamma, \Delta)$: $\gamma = 1, \Delta \in [0, 2]\}$. Since $\mathscr{S}(R^-) = (\cdot, +, -)$ as long as $R^- \neq 0$, it follows that $\lambda_2(R^-)$ and $\lambda_3(R^-)$ are always real.

4.4. *Symmetric phase drift solutions*

To complete the description of the global dynamics of solutions to (1.2) for nonzero shear, we redirect our attention to the symmetric solutions to (1.2). Again we assume that $\kappa = 1$. Here we are interested in the existence, uniqueness and stability of symmetric *running solutions*, that is, nonconstant solutions $\phi = \phi(t)$, $\rho = \rho(t)$ to (4.1) which satisfy $\dot{\phi} \neq 0$ together with

$$\phi(t + T) = \phi(t) + 2\pi, \qquad \rho(t + T) = \rho(t)$$

on $\mathbb{R}$ for some $T > 0$. A running solution will be called a *phase-drift solution* if it also satisfies

$$\rho(t) \geq \rho_0 > 0$$

on $\mathbb{R}$ for some $\rho_0 > 0$. We are mainly interested in phase-drift solutions, but their analysis requires an understanding of the behavior of running solutions with $\rho \equiv 0$. On any running solution, one Floquet multiplier is always equal to 1, while the other is given by

$$m \equiv \exp\left(\int_0^T \left[1 - \gamma - 3\rho^2(t) - \gamma \cos \phi(t) \right] dt \right).$$

In proposition 4.3 we give a simple criterion for the nonexistence of phase-drift solutions, and in propositions 4.4 and 4.5 we use fixed point arguments to prove the existence of phase-drift solutions in certain regions of parameter space. The stability and uniqueness of phase-drift solutions is addressed in proposition 4.6 and corollary 4.7, which show that in a certain parameter region every phase-drift solution is asymptotically stable and therefore unique. The main analytical result in this section is proposition 4.9, in which we study the coexistence and noncoexistence of phase-drift solutions with phase-locked saddle–nodes. In contrast to the zero-shear case which we analyzed in section 3, here the phase-locked saddle–nodes do not necessarily occur *on* the phase-drift solutions. This leads to the existence of parameter domains in which stable phase lock and stable phase drift coexist. Although the existence of these domains is a consequence of our analysis, we are forced to rely on numerical observations in order to complete the global picture. Thus, we conclude this section with a series of global bifurcation diagrams (figs. 15, 16 and 18) in which we synthesize our analytical and numerical studies.

Proposition 4.3. There exists no phase drift solution to (4.1) if $(\gamma, \Delta) \in \mathrm{N}$, where

$$\mathrm{N} \equiv \left\{ (\gamma, \Delta) : \gamma \geq \max\left(\tfrac{1}{2}(\Delta + \nu), -\tfrac{1}{2}\Delta \right), \Delta \in \mathbb{R} \right\}.$$

Proof. If $\rho > 1$ then

$$\dot{\rho} = \rho\left(1 - \gamma - \rho^2 + \gamma \cos \phi\right) < \gamma(\cos \phi - 1) \leq 0.$$

On any phase drift solution to (4.1) ρ is periodic, so it follows that ρ must take its values in $(0, 1]$. Moreover, since $|\dot{\phi}| > 0$ on a phase drift solution, it must pass through the rectangle $[0, 2\pi] \times (0, 1]$ in finite time, entering and exiting on the lateral boundaries. Thus there can be no phase drift solution if the $\dot{\phi}$–null cline

$$\rho^2 = \frac{1}{\nu}(2\gamma \sin \phi - \Delta) \tag{4.12}$$

intersects both the line $\rho = 0$ and the line $\rho = 1$. Since

$$-\frac{1}{\nu}(2\gamma + \Delta) \leq \frac{1}{\nu}(2\gamma \sin \phi - \Delta) \leq \frac{1}{\nu}(2\gamma - \Delta),$$

both of these intersections occur precisely when $(\gamma, \Delta) \in \mathrm{N}$. □

For $\gamma = 0$ there is a running solution $Z_{0\Delta}$ to (4.1) given by

$$\phi(t) = \Delta t + \phi_0, \qquad \rho(t) \equiv 0.$$

This solution extends to $Z_{\gamma\Delta}$ given by $\phi = \phi(t)$, $\rho(t) \equiv 0$ where

$$\dot{\phi} = \Delta - 2\gamma \sin\phi, \qquad \phi(0) = \phi_0$$

provided that $\gamma < \frac{1}{2}|\Delta|$. On $Z_{\gamma\Delta}$, $m = \exp[(1-\gamma)T]$ so that $Z_{\gamma\Delta}$ is asymptotically stable for $\gamma > 1$ and unstable for $\gamma \in [0,1)$.

For $\gamma = 0$ and $\Delta \neq -\nu$ there is also a phase drift solution $\mathscr{P}_{0\Delta}$ given by

$$\phi(t) = (\Delta + \nu)t + \phi_0, \qquad \rho(t) \equiv 1.$$

Note that $\dot{\rho} = \rho(1-\rho^2)$ so that $\mathscr{P}_{0\Delta}$ is the unique phase-drift solution to (4.1) for $\gamma = 0$ and is asymptotically stable. Indeed, it attracts everything in the half-space $\rho \geq 0$ except the line $\rho = 0$. Using standard local theory [29] we can extend $\mathscr{P}_{0\Delta}$ to a stable phase-drift solution $\mathscr{P}_{\gamma\Delta}$ for sufficiently small $\gamma > 0$. Here we will use the specific features of our system to get a more global extension.

Proposition 4.4. There exists a phase-drift solution to (4.1) for all $(\gamma, \Delta) \in A_1 \cup A_2$, where

$$A_1 = \{(\gamma, \Delta): 0 \leq \gamma < \min(\tfrac{1}{2}\Delta, 1), \Delta \in \mathbb{R}^+\}$$

and

$$A_2 = \{(\gamma, \Delta): 0 \leq \gamma < \min(l_\nu(\Delta), \tfrac{1}{2}|\Delta|, 1), \Delta \in \mathbb{R}^-\} \setminus \{(0, -\nu)\}.$$

Proof. As we observed above, there is always a phase drift solution $\mathscr{P}_{0\Delta}$ for $\gamma = 0$ and $\Delta \neq -\nu$. It therefore suffices to consider the case $\gamma > 0$.

For $0 < \gamma < \frac{1}{2}\Delta$, $\dot{\phi} > 0$ everywhere in the half-space $\rho \geq 0$. For $\gamma \in [0,1)$, $Z_{\gamma\Delta}$ is unstable; thus, for any sufficiently small $\rho_1 > 0$, if we follow the trajectory of (4.1) through $(2\pi, \rho_1)$ backwards in time until the time t_0 at which $\phi(t_0) = 0$, then $\rho_0 \equiv \rho(t_0) < \rho_1$. On the other hand, $\dot{\phi}(t) > 0$ and $\rho(t) < 1$ for all $t \in \mathbb{R}^+$ on the trajectory of (4.1) through $(0,1)$. Thus under the flow of (4.1), the segment $[\rho_0, 1]$ is mapped modulo 2π into its interior (fig. 8a.) The flow map therefore has a fixed point on $(\rho_0, 1)$. Since there are no rest points, a standard argument shows that fixed points of the flow map correspond to phase drift solutions. Thus, we are done for $(\gamma, \Delta) \in A_1$.

For $(\gamma, \Delta) \in A_2$ with $\Delta \in (-\nu, 0)$, the $\dot{\phi}$–null cline (4.12) lies between the $\dot{\rho}$–null clines $\rho = 0$ and

$$\rho^2 = 1 + \gamma(\cos\phi - 1). \tag{4.13}$$

This is true because, at $\phi = 0$, the point of $\dot{\phi} = 0$ is $\bar{\rho}_0 \equiv \sqrt{-\Delta/\nu}$, and $0 < \bar{\rho}_0 < 1$. There are no rest points of (4.1) for $(\gamma, \Delta) \in A_2$, so the curves $\dot{\phi} = 0$, $\dot{\rho} = 0$ may not cross. Since the vector field on the $\dot{\phi}$–null cline is vertically upward, $\dot{\phi} > 0$ and $\rho^2 > (2\gamma \sin\phi - \Delta)/\nu$ on the trajectory of (4.1) through $(0, \bar{\rho}_0)$. Moreover, $\dot{\phi} > 0$ and $\rho < 1$ in $\mathbb{R}^+$ on the trajectory of (4.1) through $(0,1)$. Thus the flow of (4.1) maps (modulo 2π) the segment $[\bar{\rho}_0, 1]$ into its interior and there exists a phase drift solution (fig. 8b).

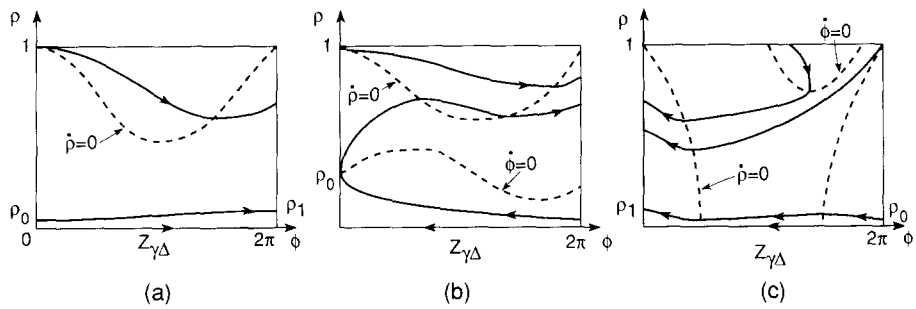

Fig. 8. Cases of proof of proposition 4.4. (a) $(\gamma, \Delta) \in A_1$; (b) $(\gamma, \Delta) \in A_2, \Delta \in (-\nu, 0)$; (c) $(\gamma, \Delta) \in A_2, \Delta < -\nu$. In each of the cases, the null clines $\dot{\rho} = 0$ and $\dot{\phi} = 0$ do not intersect.

For $(\gamma, \Delta) \in A_2$ with $\Delta < -\nu$, the $\dot{\phi}$–null cline lies strictly above the $\dot{\rho}$–null cline (4.13). Hence the vector field points vertically downward on the $\dot{\phi}$–null cline. On the trajectory of (4.1) through $(2\pi, 1)$, $\dot{\phi} < 0$ and $\rho < 1$ in $\mathbb{R}^+$. Since $\dot{\phi} < 0$ in the neighborhood of the unstable running solution $Z_{\gamma,\Delta}$, for sufficiently small $\rho_0 > 0$, the trajectory of (4.1) through $(2\pi, \rho_0)$ satisfies $\rho_1 \equiv \rho(t_0) > \rho_0$ at the time t_0 for which $\phi(t_0) = 0$. Thus the flow maps (modulo 2π) the segment $[\rho_0, 1]$ into its interior and there exists a phase drift solution (fig. 8c). □

In order to analyze the evolution of phase drift solutions in the parameter space, we must first analyze the evolution of the running solution $\rho = 0$. This analysis is independent of ν and hence could have been done in section 3. Since it is not relevant to the conclusions of section 3, we include it here where it is relevant. Throughout the discussion we will consider $\phi \in S^1$, and so not distinguish between angles which differ by multiples of 2π.

For parameter points with $\gamma = \frac{1}{2}\Delta$ and $\Delta > 0$ there is a saddle–node bifurcation on the line $\rho = 0$ at $\phi = \pi/2$. Similarly, for parameter points with $\gamma = -\frac{1}{2}\Delta$ and $\Delta < 0$ there is a saddle–node bifurcation on the line $\rho = 0$ at $\phi = 3\pi/2$. At these bifurcations, the running solution $Z_{\gamma\Delta}$ becomes a homoclinic orbit connecting the saddle–nodes. For $\gamma > \frac{1}{2}|\Delta|$ the saddle–nodes split into a pair of rest points $(\phi^{\pm}, 0)$ with

$$\phi^+ = \begin{cases} \arcsin(\Delta/2\gamma) & \text{for } \Delta \geq 0, \\ 2\pi + \arcsin(\Delta/2\gamma) & \text{for } \Delta < 0. \end{cases} \qquad \phi^- = \pi - \arcsin(\Delta/2\gamma),$$

The stability of these rest points is determined by the eigenvalues of the differential of the right-hand side of (4.1). These are

$$\lambda_1(\phi) = a + \gamma\cos\phi, \qquad \lambda_2(\phi) = -2\gamma\cos\phi.$$

Since $\cos\phi^+ = \sqrt{\gamma^2 - \frac{1}{4}\Delta^2}\,/\gamma$, it follows that $\lambda_2(\phi^+) < 0$ for all $\gamma > \frac{1}{2}|\Delta|$. On the other hand, using (4.6), we have

$$\begin{aligned} \lambda_1(\phi^+) > 0 \quad & \text{in } \{(\gamma, \Delta) : \gamma > \tfrac{1}{2}|\Delta|, |\Delta| < 2\} \\ < 0 \quad & \text{in } \{(\gamma, \Delta) : \tfrac{1}{2}|\Delta| < \gamma < k(\Delta), |\Delta| > 2\} \\ > 0 \quad & \text{in } \{(\gamma, \Delta) : \gamma > k(\Delta), |\Delta| > 2\}. \end{aligned}$$

For $|\Delta| < 2$, $(\phi^+, 0)$ is a saddle point with stable manifold along the line $\rho = 0$ and unstable manifold perpendicular to $\rho = 0$. For $|\Delta| > 2$, $(\phi^+, 0)$ is a stable node for $\frac{1}{2}|\Delta| < \gamma < k(\Delta)$ and a saddle point for

$\gamma > k(\Delta)$. The bifurcation at $(\phi^+, 0)$ for $\gamma = k(\Delta)$ corresponds to the birth of the R^+ branch of phase-locked solutions for $\Delta > 2$ or $\Delta < \Delta_{-2}$, and to the disappearance of the R^- branch for $\Delta_{-2} < \Delta < -2$ (see section 4.1).

Since $\cos\phi^- = -\sqrt{\gamma^2 - \frac{1}{4}\Delta^2}/\gamma$, it follows that $\lambda_2(\phi^-) > 0$ for all $\gamma > \frac{1}{2}|\Delta|$. Moreover

$$\begin{aligned} \lambda_1(\phi^-) &< 0 \quad \text{in } \{(\gamma, \Delta): \gamma > \tfrac{1}{2}|\Delta|, |\Delta| > 2\}, \\ &> 0 \quad \text{in } \{(\gamma, \Delta): \tfrac{1}{2}|\Delta| < \gamma < k(\Delta), |\Delta| < 2\}, \\ &< 0 \quad \text{in } \{(\gamma, \Delta): \gamma > k(\Delta), |\Delta| < 2\}. \end{aligned}$$

Thus for $|\Delta| > 2$, $(\phi^-, 0)$ is a saddle point. For $|\Delta| < 2$ it changes from an unstable node to a saddle as γ increases from $\frac{1}{2}|\Delta|$ through $k(\Delta)$. The bifurcation at $(\phi^-, 0)$ for $\gamma = k(\Delta)$ when $|\Delta| < 2$ corresponds to the disappearance of the R^- branch of symmetric phase-locked solutions.

Using some of the properties of the rest points on $\rho = 0$ for $\gamma > \frac{1}{2}|\Delta|$, we extend the existence result in proposition 4.4 to a somewhat larger parameter domain, specifically up to the curve

$$\begin{aligned} p_\nu(\Delta) &\equiv l_\nu(\Delta) \quad \text{for } \Delta \in [\Delta_{-2}, \Delta_2], \\ &\equiv k(\Delta) \quad \text{for } \Delta \in (-\infty, \Delta_{-2}) \cup (\Delta_2, \infty). \end{aligned}$$

Note that $\gamma = p_\nu(\Delta)$ is the curve along which the R^+ symmetric phase-locked solutions are born in a saddle–node bifurcation involving either the R^- solution branch if $\Delta \in [\Delta_{-2}, \Delta_2]$ or the $(\phi^+, 0)$ solution if $\Delta \notin [\Delta_{-2}, \Delta_2]$. Moreover, the curves $\gamma = \frac{1}{2}|\Delta|$ and $\gamma = l_\nu(\Delta)$ intersect at

$$\Delta = \Delta^* \equiv -\nu(\sqrt{s} - \nu)/(\sqrt{s} - \nu + 2).$$

Proposition 4.5. There exists a phase-drift solution to (4.2) for all $(\gamma, \Delta) \in \mathrm{B}$, where

$$\mathrm{B} \equiv \{(\gamma, \Delta): \tfrac{1}{2}|\Delta| \le \gamma < p_\nu(\Delta), \Delta^* < \Delta < 2\}.$$

Proof. For $(\gamma, \Delta) \in \mathrm{B}$ the only rest points of (4.1) in the half-space $\rho \ge 0$ are the points $(\phi^\pm, 0)$ discussed above. In addition, the $\dot\phi$–null cline lies completely below the $\dot\rho$–null cline (4.13), so the vector field points vertically upward on the $\dot\phi$–null cline and $\dot\phi > 0$ everywhere above it. For $\Delta > 0$, $\dot\phi > 0$ and $0 < \rho < 1$ for all $t \in \mathbb{R}$ on the unstable manifold of $(\phi^+, 0)$. On the trajectory of (4.1) through $(\phi^+, 1)$ we also have $\dot\phi > 0$ and $0 < \rho < 1$. Thus the phase portrait (modulo 2π) is as shown in fig. 9a. From similar considerations one can conclude that the phase portrait for $\Delta \in (\Delta^*, 0]$ is as shown in fig. 9b. In both cases the existence of a phase drift solution is clear from the standard fixed point argument. □

We now turn to the questions of uniqueness and stability of phase drift solutions. For $\nu = 0$, the Floquet multipliers could be calculated explicitly; for $\nu \neq 0$ the argument is less simple.

Proposition 4.6. Let

$$\mathrm{C} \equiv \{(\gamma, \Delta): 0 \le \gamma < l_\nu(\Delta), \Delta \in \mathbb{R}\}.$$

If $\mathscr{P}$ is any phase drift solution to (4.1) for $(\gamma, \Delta) \in \mathrm{Cl}\,\mathrm{C}$, then $\mathscr{P}$ is asymptotically stable.

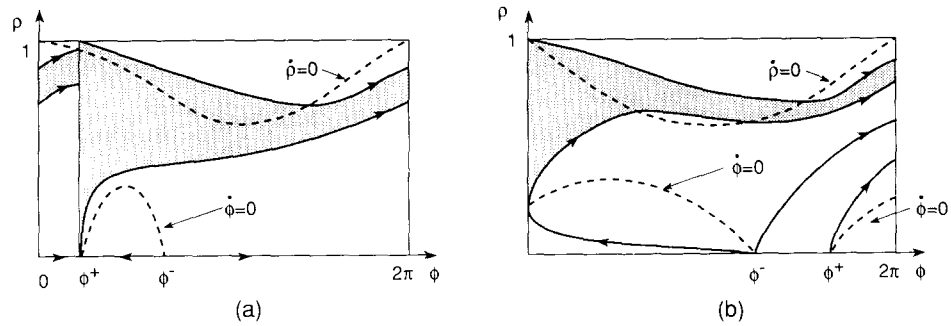

Fig. 9. Cases of proof of proposition 4.5. (a) $\Delta > 0$; (b) $\Delta^* < \Delta < 0$. In both cases, the $\dot{\phi} = 0$ null cline lies below the $\dot{\rho} = 0$ null cline.

Remark. By continuity, asymptotic stability extends a little beyond Cl C.

Corollary 4.7. For any $(\gamma, \Delta) \in C$ there exists at most one phase-drift solution to (3.1).

Proof of corollary 4.7. For $(\gamma, \Delta) \in C$ there are no rest points of (4.1) in the half-space $\rho > 0$. If $\mathscr{P}_1$ and $\mathscr{P}_2$ are two phase drift solutions to (4.1), then, by proposition 4.4, both $\mathscr{P}_1$ and $\mathscr{P}_2$ are asymptotically stable. There must therefore be an unstable object between $\mathscr{P}_1$ and $\mathscr{P}_2$. However, this is impossible since there are no rest points in $\rho > 0$ and no unstable phase drift solutions. □

Proof of proposition 4.6. Let $\mathscr{P}$: $\phi = \phi_0(t)$, $\rho = \rho_0(t)$ be a phase-drift solution to (4.1). Then, in particular, $\dot{\phi}_0(t) \neq 0$ in $\mathbb{R}$. We claim that $\dot{\phi}_0 > 0$ (< 0) if and only if $\Delta + \nu > 0$ (< 0). To prove this we first consider the case $(\gamma, \Delta) \in C$, in which there are no rest points for (4.1) in the open half-space $\rho > 0$. In this case the $\dot{\phi}$–null cline (4.12) and the $\dot{\rho}$–null cline (4.13) do not intersect. In particular, $\dot{\phi} > 0$ (< 0) on the $\dot{\rho}$–null cline (4.13) if and only if it lies above (below) the $\dot{\rho}$–null cline. The phase drift solution $\mathscr{P}$ must intersect the $\dot{\rho}$–null cline (4.13). Therefore, $\dot{\phi}_0 > 0$ (< 0) if and only if (4.13) lies above (below) (4.12). Finally, the necessary and sufficient condition for (4.13) to lie above (below) (4.12) is $\Delta + \nu > 0$ (< 0). It is easy to see that the above argument remains valid for $(\gamma, \Delta) \in$ Cl C provided that the saddle–nodes which arise for (γ, Δ) on $\gamma = l_\nu(\Delta)$ do not break $\mathscr{P}$.

We now change coordinates in a neighborhood of $\mathscr{P}$. For $\Delta + \nu \neq 0$, $|\dot{\phi}_0|$ is bounded away from 0. Hence, there is a neighborhood $\mathscr{N}$ of $\mathscr{P}$ in ϕ, ρ space in which $|\Delta + \nu\rho_0^2 - 2\gamma \sin\phi|$ is bounded away from 0. For $(\phi, \rho) \in \mathscr{N}$ we take ϕ as independent variable and write (4.1) in the form

$$\frac{\mathrm{d}}{\mathrm{d}\phi} \log \rho = \frac{a + \gamma \cos\phi - \rho^2}{\Delta - 2\gamma \sin\phi + \nu\rho^2}, \tag{4.14}$$

where, with a slight abuse of notation, we have set $\rho = \rho(\phi)$. By continuity with respect to initial data, any solution starting in $\mathscr{N}$ sufficiently close to $\mathscr{P}$ stays in $\mathscr{N}$ for $\phi \in [-2\pi, 2\pi]$.

If $(\phi, \rho(\phi)) \in \mathcal{N}$ then

$$\frac{\mathrm{d}}{\mathrm{d}\phi}\log\frac{\rho}{\rho_0} = (\rho_0^2 - \rho^2)\mathcal{F}(\phi, \rho, \gamma, \Delta), \tag{4.15}$$

where

$$\mathcal{F}(\phi, \rho, \gamma, \Delta) \equiv \frac{\nu a + \Delta + \nu\gamma\cos\phi - 2\gamma\sin\phi}{(\Delta - 2\gamma\sin\phi + \nu\rho_0^2)(\Delta - 2\gamma\sin\phi + \nu\rho^2)}.$$

Observe that the sign of $\mathcal{F}$ is determined by the sign of

$$Q(\phi, \gamma, \Delta) \equiv \nu a + \Delta + \nu\gamma\cos\phi - 2\gamma\sin\phi.$$

As a function of ϕ, Q achieves its minimum value at $\phi = \pi + \arctan(-2/\nu)$, its maximum value at $\phi = 2\pi + \arctan(-2/\nu)$, and satisfies

$$\nu a + \Delta - \gamma\sqrt{s} \le Q(\phi, \gamma, \Delta) \le \nu a + \Delta + \gamma\sqrt{s}.$$

The left-hand equality holds only for $\phi = \pi + \arctan(-2/\nu)$ and the right-hand equality holds only if $\phi = 2\pi + \arctan(-2/\nu)$. It is not difficult to verify that

$$\nu a + \Delta - \gamma\sqrt{s} \ge 0 \quad \text{if and only if } \gamma \le \tfrac{1}{4}(\Delta + \nu)(\sqrt{s} - \nu) \tag{4.16}$$

and

$$\nu a + \Delta + \gamma\sqrt{s} < 0 \quad \text{if and only if } \gamma \le -\tfrac{1}{4}(\Delta + \nu)(\sqrt{s} + \nu). \tag{4.17}$$

Note that the right-hand sides of (4.16), (4.17) give the formulas (4.5) for $I(\Delta)$ in the two cases $\Delta + \nu > 0$, $\Delta + \nu < 0$.

Suppose first that $\dot{\phi}_0 > 0$. Then we want to show that $|\rho(\phi) - \rho_0(\phi)| \to 0$ as $\phi \to \infty$ provided that $(\gamma, \Delta) \in \mathrm{Cl}\,\mathrm{C}$ and $|\rho(0) - \rho_0(0)|$ is sufficiently small. To do this we consider the Poincaré map of $\rho_0(\phi)$ and show that it has an attracting fixed point. Since $\dot{\phi}_0 > 0$, it follows that $\Delta + \nu > 0$. Then (4.16) implies that $\mathcal{F}(\phi, \rho, \gamma, \Delta) \ge 0$ in $\mathcal{N} \times \mathrm{Cl}\,\mathrm{C}$, with equality for at most one value of ϕ. In terms of $\zeta \equiv \log\rho/\rho_0$, (4.15) becomes

$$\frac{\mathrm{d}\zeta}{\mathrm{d}\phi} = \rho_0^2(1 - \mathrm{e}^{2\zeta})\mathcal{F}^*(\phi, \zeta, \gamma, \Delta), \tag{4.18}$$

where $\mathcal{F}^*(\phi, \zeta, \gamma, \Delta) \equiv \mathcal{F}(\phi, \rho_0\,\mathrm{e}^{\zeta}, \gamma, \Delta)$. Then $\zeta \equiv 0$ is a solution of (4.18) and the derivative of the right-hand side of (4.19) with respect to ζ, evaluated at $\zeta = 0$, is strictly negative. It follows that the linearization of the Poincaré map has an eigenvalue strictly less than 1.

If $\dot{\phi}_0 < 0$ then we want to show that $|\rho(\phi) - \rho_0(\phi)| \to 0$ as $\phi \to -\infty$ provided that $(\gamma, \Delta) \in \mathrm{Cl}\,\mathrm{C}$ and $|\rho(0) - \rho_0(0)|$ is sufficiently small. Since $\dot{\phi}_0 < 0$ it follows that $\nu + \Delta < 0$. Then (4.17) implies that

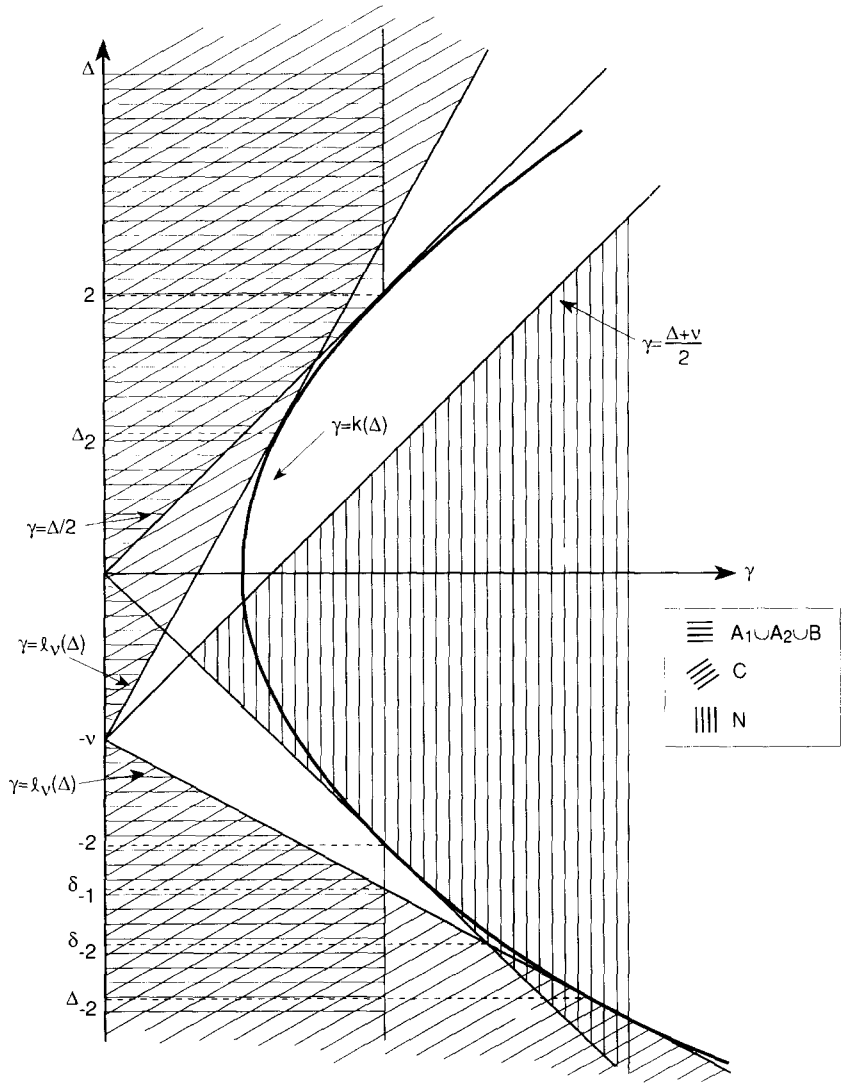

Fig. 10. Parameter domains for phase drift in symmetric ρ, ϕ flow. In $A_1 \cup A_2 \cup B$, there is a phase drift solution for (4.1). In C, any phase drift solution that exists must be unique and stable. Note that C and $A_1 \cup A_2 \cup B$ overlap, but do not coincide. In N, there are no phase drift solutions.

$\mathcal{F}(\phi, \rho, \gamma, \Delta) \leq 0$ in $\mathcal{N} \times \mathrm{Cl}\, C$ with equality for at most one value of ϕ. If we replace ϕ by $-\phi$ in (4.18), the proof of stability proceeds exactly as in the previous case. □

Thus far we have shown the existence of a phase-drift solution in the parameter domain $A_1 \cup A_2 \cup B$, and the nonexistence of phase-drift solutions in the parameter domain N (fig. 10). Moreover, we have shown that in the parameter domain C any phase-drift solution must be stable and unique. Our next result gives some information about the nature of phase drift solutions in still another subset of the parameter space. A phase drift solution $\mathcal{P}$ will be called *minimal* if there are no phase drift solutions between $\mathcal{P}$ and the line $\rho = 0$.

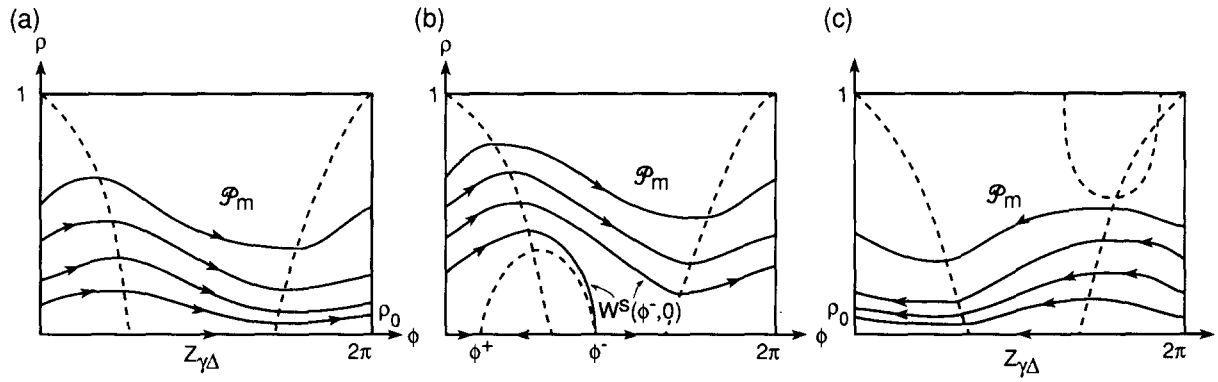

Fig. 11. Cases in the proof of proposition 4.8. The minimal phase drift solution is labelled $\mathcal{P}_m$. (a) $\Delta > 2, 1 < \gamma < \frac{1}{2}\Delta$; (b) $\Delta > 2, \gamma > \frac{1}{2}$; (c) $\Delta < -2, 1 < \gamma < \frac{1}{2}|\Delta|$. In each case, a region is identified with no rest points between a pair of orbits.

Proposition 4.8. Let

$$M \equiv \{(\gamma, \Delta): \gamma \in (1, \infty), \Delta \in (-\infty, -2) \cup (2, \infty)\}.$$

If there is a phase-drift solution to (4.1) for $(\gamma, \Delta) \in M$ then the minimal phase-drift solution $\mathcal{P}_m$ is unstable from below.

Proof. If $\gamma \in (1, \frac{1}{2}\Delta)$ for $\Delta > 2$, then $Z_{\gamma\Delta}$ is stable. Let $\rho_0 \in (0,1)$ be such that $\rho \to 0$ on the forward orbit through $(2\pi, \rho_0)$. Since there are no rest points in the upper half-space $\rho \geq 0$ the backward orbit through $(2\pi, \rho_0)$ must approach the minimal phase-drift solution $\mathcal{P}_m$ as $t \to -\infty$ (fig. 11a). Thus $\mathcal{P}_m$ is unstable from below. If $\gamma > \frac{1}{2}\Delta$ for $\Delta > 2$ then $Z_{\gamma\Delta}$ no longer exists and there are rest points $(\phi^{\pm}, 0)$ on $\rho = 0$. In particular, $(\phi^-, 0)$ is a saddle point whose stable manifold $W^s(\phi^-, 0)$ is in the set where $\dot{\phi} > 0$. Since there are no rest points in the half-space $\rho > 0$, $W^s(\phi^-, 0)$ approaches $\mathcal{P}_m$ as $t \to \infty$ and it follows that $\mathcal{P}_m$ is unstable from below (fig. 11b). If $\Delta < -2$ then, in view of proposition 4.1, there exist phase-drift solutions only for (γ, Δ) in the subset of M characterized by $1 < \gamma < \frac{1}{2}|\Delta|$. In this case the phase portrait is as shown in fig. 11c. Since $Z_{\gamma\Delta}$ is stable and there are no rest points in $\rho \geq 0$ on or below $\mathcal{P}_m$, it is clear that $\mathcal{P}_m$ is unstable. □

Remarks

(1) For $\nu = 0$ the parameter domains in propositions 4.3 to 4.8 fit together neatly to reconfirm the picture obtained directly in section 3. Specifically, there exists a symmetric phase-drift solution which is unique and stable in the parameter domain $\{(\gamma, \Delta): 0 \leq \gamma < \min(\frac{1}{2}|\Delta|, 1), \Delta \in \mathbb{R}\} = A_1 \cup A_2 \cup B \subset C$, and there exists no phase-drift solution in $\{(\gamma, \Delta): \gamma \geq \frac{1}{2}|\Delta|, \Delta \in \mathbb{R}\} = N$. Moreover in the remainder of the parameter space, $\{(\gamma, \Delta): 1 < \gamma < \frac{1}{2}|\Delta|, |\Delta| > 2\} \subset M$, the minimal phase drift solution $\mathcal{P}_m$, if it exists, must be unstable from below. Actually it is not difficult to show that *for $\nu = 0$ there can be no phase-drift solution at all in this part of the parameter space.* If there exists a phase-drift solution, then there exists a minimal one $\mathcal{P}_m$, and $\mathcal{P}_m$ is unstable from below. Let $\mathcal{P}_m$ be given by $\rho = \rho_m(\phi)$ and assume that $\Delta > 2$. Since $\rho_m(2\pi) = \rho_m(0)$, it follows by integrating (4.14) that

$$0 = A - F[\rho_m],$$

where

$$A = A(\gamma, \Delta) \equiv \int_0^{2\pi} \frac{a + \gamma \cos\phi}{\Delta - 2\gamma \sin\phi}\, d\phi,$$

$$F[\rho] = F_{\gamma\Delta}[\rho] \equiv \int_0^{2\pi} \frac{\rho^2}{\Delta - 2\gamma \sin\phi}\, d\phi.$$

Let $\rho = \rho(\phi, \rho_0)$ denote the solution to (4.14) through $(0, \rho_0)$ where $\rho_0 < \rho_m(0)$. Then $\rho(\phi, \rho_0) < \rho_m(\phi)$ on $[0, 2\pi]$. Moreover, in view of the instability of $\mathscr{P}_m$, ρ_0 sufficiently close to $\rho_m(0)$ implies that $\rho(2\pi, \rho_0) < \rho_0$. Now integrate (4.14) on $\rho = \rho(\phi, \rho_0)$ to obtain the contradiction

$$0 > \log \rho(2\pi, \rho_0) - \log \rho_0 = A - F[\rho] > A - F[\rho_m] = 0.$$

(2) For $\nu > 0$ the parameter domains in propositions 4.3–4.8 do not fit together so neatly and there are several gaps (cf. fig. 10). As we will see presently, parts of the gaps for $\gamma < 1$ are essential since there are open subsets of the parameter space where stable phase drift coexists with stable phase lock. The boundaries of these subsets are determined by certain global bifurcations which are described below. For the most part these global bifurcations are beyond the reach of the rather crude analysis employed here and we will ultimately have to rely on numerical observations. However, there still remains some further information which can be gotten analytically.

Along the curve $\gamma = l_\nu(\Delta)$ for $\Delta \in (\Delta_{-2}, \Delta_2)$ there are saddle-node bifurcations of rest points of (4.1), with a codimension-2 bifurcation (Bogdanov–Takens point) occurring at (γ_1, Δ_1). From the general theory [28, p. 371] we know that the local picture near (γ_1, Δ_1) is as shown in fig. 12. The curve of Hopf bifurcations which is labeled (hopf) in fig. 12 has already been identified in section 4.3 and is given by $\Delta = h_\nu^+(\gamma)$, where $h_\nu^+(\gamma)$ is defined by (4.8). We do not have an analytic expression for the curve of

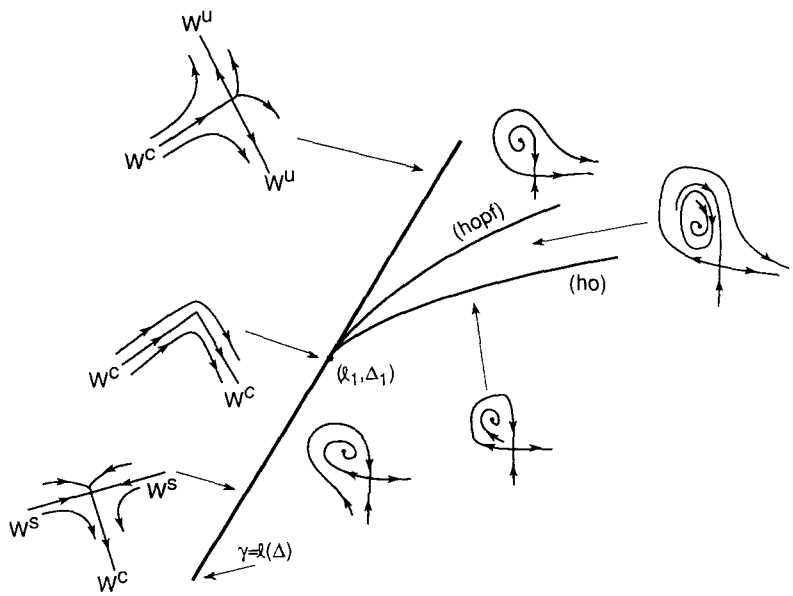

Fig. 12. The local flow near a degenerate saddle-node ("Bogdanov–Takens point").

homoclinic bifurcations which is labeled (ho) in fig. 12; however, it is tangent to the Hopf curve at (γ_1, Δ_1). In order to see how the local picture in fig. 12 interacts with our particular global configuration, we begin by examining how the phase portraits change as we move along the curve $\gamma = p_\nu(\Delta)$ in parameter space.

For $\Delta \in (\Delta_1, \Delta_2)$ the saddle–nodes which occur in the curve $\gamma = l_\nu(\Delta) = p_\nu(\Delta)$ combine a saddle with an *unstable* node. The local flow near such a saddle–node is shown schematically in fig. 12. The unstable manifold W^u is tangent to the eigenvector corresponding to the positive eigenvalue, and the center manifold W^c is tangent to the eigenvector corresponding to the zero eigenvalue. For $\Delta < \Delta_1$ the saddle–nodes which occur on $\gamma = l_\nu(\Delta)$ combine a saddle with a *stable* node. Again, the local flow is shown schematically in fig. 12. Here the stable manifold W^s is tangent to the eigenvector corresponding to the negative eigenvalue. In the degenerate case $\Delta = \Delta_1$, there are two zero eigenvalues and the manifolds labeled W^c are tangent to the corresponding eigenvectors. By combining these local pictures with the various other features of the flow for (γ, Δ) on $\gamma = \rho_\nu(\Delta)$ we can derive the following information about the coexistence and non-coexistence of stable phase drift and saddle–node phase lock.

If there exists a phase drift solution to (4.1), then in addition to the minimal phase drift solution $\mathscr{P}_m$ discussed above, there is a maximal phase-drift solution $\mathscr{P}_M$ characterized by the absence of phase-drift solutions between $\mathscr{P}_M$ and the line $\rho = 1$. In counting the number of phase-drift solutions we use the convention that a stable or unstable phase-drift solution has multiplicity 1 while a neutrally stable (saddle–node) phase-drift solution has multiplicity 2. The following proposition, especially part (e), will later be supplemented with numerical data.

Proposition 4.9. Assume (γ, Δ) satisfy $\gamma = \rho_\nu(\Delta)$ so that there exist saddle–node phase-lock solutions to (4.1).

(a) For $\Delta \in [\Delta_1, \Delta_2)$ there exists a phase-drift solution which is stable and unique.

(b) For $\Delta \in [\Delta_2, 2)$ there exists an odd number of phase-drift solutions with $\mathscr{P}_m$ stable from below and $\mathscr{P}_M$ stable from above.

(c) For $\Delta > 2$ there exists an even number of phase-drift solutions with $\mathscr{P}_m$ unstable from below and $\mathscr{P}_M$ stable from above.

(d) Define $\delta_{-1} \in \mathbb{R}^-$ by $l_\nu(\delta_{-1}) = 1$. Then there exist no phase-drift solutions to (4.1) for $\Delta < \delta_{-1}$.

(e) Suppose that $\Delta \in (\delta_{-1}, \Delta_1)$. If $W^c \not\equiv W^s$ and W^c approaches the saddle–node as $t \to \infty$, then there exists no phase-drift solution. If $W^c \not\equiv W^s$ and W^c does not approach the saddle–node as $t \to \infty$, then there exists a phase-drift solution which is stable and unique.

Proof

(a) If $\Delta \in (\Delta_1, \Delta_2)$ and $\Delta > 0$ then the $\dot{\phi}$–null cline and the $\dot{\rho}$–null clines are as shown in fig. 13a. The local flow near the saddle–node as shown in fig. 12 can be fit into this picture only with W^c coming from the unstable node at $(\phi^-, 0)$. All other orbits which approach the saddle–node must do so as $t \to -\infty$ and are as shown in fig. 13a. Therefore the unstable manifold $W^u(\phi^+, 0)$ from the saddle point $(\phi^+, 0)$ does not approach the saddle–node as $t \to \infty$ and, indeed, lies strictly above it and both branches of W^s. This justifies the phase portrait given in fig. 13a, from which the existence of a phase-drift solution is clear. Uniqueness and stability follow from proposition 4.6. An analogous argument justifies the phase portrait for $\Delta = \Delta_1$ (fig. 13b) and its interpretation. Similar arguments apply if $\Delta < 0$.

(b) For $\Delta \in [\Delta_2, 2)$ the saddle–node occurs at $(\phi^-, 0)$. Since no orbit in $\rho \geq 0$ approaches $(\phi^-, 0)$ as $t \to \infty$ the phase portrait is as shown in fig. 13c. At least one phase-drift solution exists in the strip between

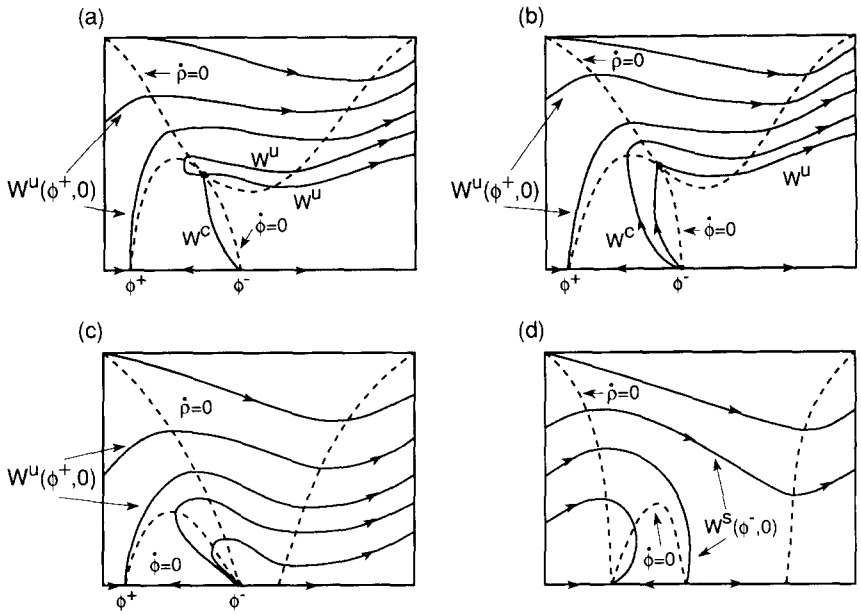

Fig. 13. Cases in the proof of prop 4.9. (a) and (b) refer to case a, (c) to case b, and (d) to case c. In each case, the saddle–node is isolated from the shaded region in the flow. This region is bounded on one side by the orbit through (0,1); on the other side it is bounded by $W^u(\phi^+,0)$ in cases a, b, c and by $W^s(\phi^-,0)$ in case d. A phase-drift solution occurs in that region. (a) $\Delta \in (\Delta_1, \Delta_2)$; (b) $\Delta = \Delta_1$; (c) $\Delta \in [\Delta_2, 2)$; (d) $\Delta > 2$.

$W^u(\phi^+,0)$ and the forward orbit through (0,1). If it is unique then it must be stable. Otherwise there must be an odd number of phase-drift solutions with $\mathscr{P}_m$ stable from below and $\mathscr{P}_M$ stable from above.

(c) For $\Delta > 2$ there is a "stable" saddle–node at $(\phi^+,0)$. Locally everything below the stable manifold $W^s(\phi^-,0)$ of the saddle point $(\phi^-,0)$ is attracted to $(\phi^+,0)$. See fig. 13d. If there exist any phase-drift solutions they must be in the strip between $W^s(\phi^-,0)$ and the forward orbit through (0,1). In that case, there must be an even number of phase-drift solutions with $\mathscr{P}_m$ unstable from below and $\mathscr{P}_M$ stable from above.

(d) Let $\delta_{-2} \in \mathbb{R}^-$ be the more negative value of δ such that $I_\nu(\delta) = \frac{1}{2}|\delta|$. Observe that $\delta_{-2} < \delta_{-1} < -2$ (cf. fig. 10). According to proposition 4.3, there exists no phase-drift solution on $\gamma = p_\nu(\Delta)$ for $\Delta \le \delta_{-2}$; hence it suffices to consider $\Delta \in (\delta_{-2}, \delta_{-1})$. However, for $\Delta \in (\delta_{-2}, \delta_{-1})$ the nonexistence of phase drift follows from propositions 4.6 and 4.7.

(e) For $\Delta \in (\delta_{-1}, \Delta_1)$ the local flow near the saddle–node is shown schematically in fig. 12. Fig. 14 shows various possible global phase portraits incorporating this local flow. Row (b) contains phase portraits for the separating case $W^c \equiv W^s$, which is not included in the statement of proposition 4.9. In fig. 14a, $W^c \neq W^s$ and W^c does not approach the saddle–node as $t \to \infty$. For $\Delta > -\nu$ there is at least one phase-drift solution in the strip between W^c and the forward orbit through (0,1). By proposition 4.6 every phase-drift solution is stable and this implies uniqueness. For $\Delta < -\nu$ we use the fact that $Z_{\gamma\Delta}$ is unstable. Thus there exists a $\rho_0 > 0$ such that the solution $\rho = \rho(\phi, \rho_0)$ of (4.14) through $(2\pi, \rho_0)$ satisfies $\rho(0, \rho_0) > \rho_0$. There is a phase-drift solution in the strip between W^c and $\rho = \rho(\phi, \rho_0)$. Stability and uniqueness again follow from proposition 4.6. In fig. 14c, $W^c \neq W^s$ and W^c approaches the saddle–node as $t \to \infty$. For $\Delta > -\nu$ everything below W^s is attracted to the saddle–node. Thus if a phase-drift solution exists it must be in the strip between W^s and the forward orbit through (0,1). However, if there exist

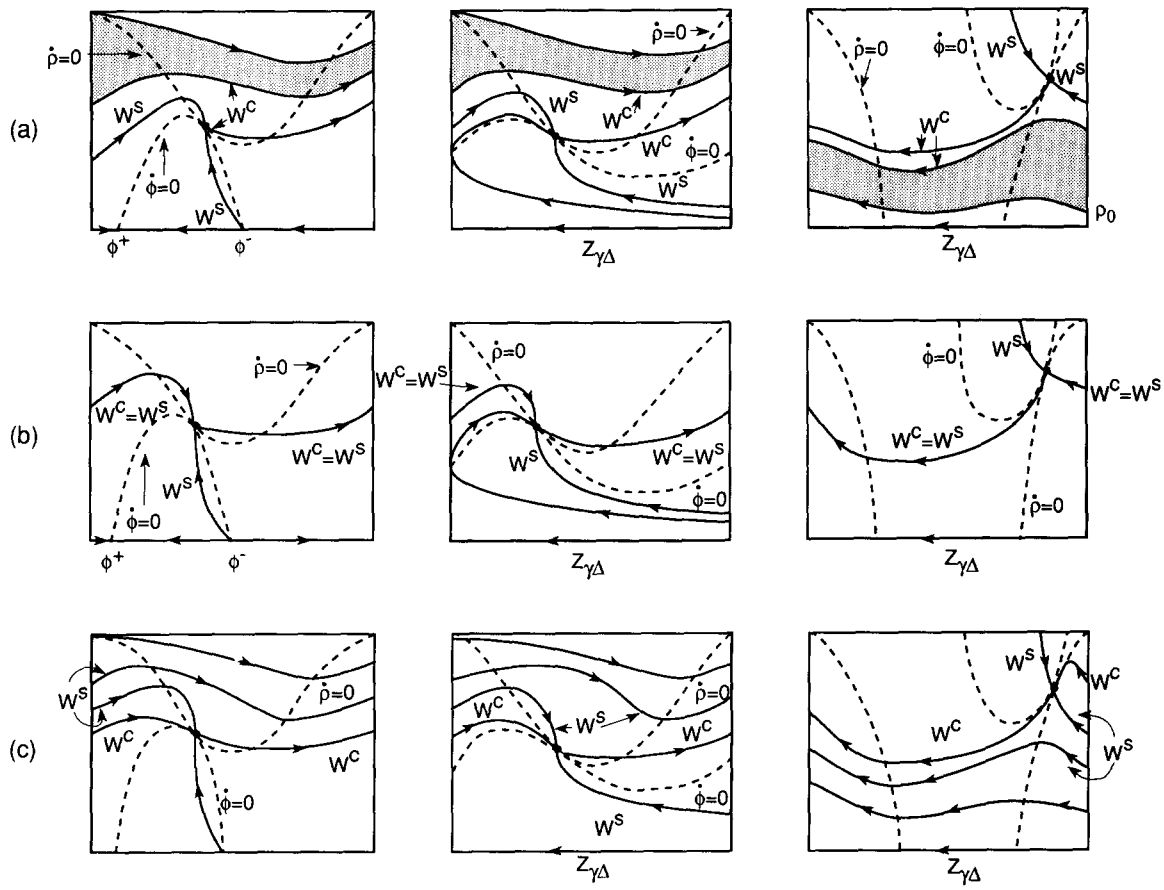

Fig. 14. Three different sets of possible global phase portraits for the symmetric ρ, ϕ flow. In the three pictures of case (a), there is a stable phase drift; in those of case (b), there is a homoclinic orbit; in those of (c), there is no phase drift. The only difference among the various columns is in the relative positions of the null clines; from left to right: $\Delta > 0$, $-\nu < \Delta < 0$, $\Delta < -\nu$.

phase-drift solutions then $\mathscr{P}_m$ must be unstable from below in contradiction to proposition 4.6. Therefore we conclude that there are no phase-drift solutions and that everything in the half-space $\rho > 0$ is attracted to the saddle–node. For $\Delta < -\nu$, the saddle–node attracts everything above W^s. If there is a phase-drift solution it must lie between W^s and $Z_{\gamma\Delta}$, and $\mathscr{P}_M$ must be unstable from above. Since this contradicts proposition 4.6 we conclude that there is no phase-drift solution and the saddle–node attracts everything in the half-space $\rho > 0$. □

In order to continue our description of the behavior of the phase-drift solution to (4.1) as the parameters are changed, we must now turn to the results of our numerical investigations. The detailed calculations which we report were made for $\nu = 0.8$. However, the main qualitative features of the results seem to be independent of the value of $\nu > 0$.

In parts (b) and (c) of proposition 4.9 we do not rule out the possibility of more than one phase-drift solution. However, in our numerical studies we have seen no evidence for nonuniqueness. On the contrary, we find that *there is a unique stable drift solution on* $\gamma = l_\nu(\Delta)$ *for* $\Delta \in [\Delta_2, 2]$ *and that there are no phase-drift solutions on* $\gamma = l_\nu(\Delta)$ *for* $\Delta > 2$. *Moreover, at the transition point* $\gamma = 1$, $\Delta = 2$ *there is no phase-drift solution and everything in the half-space* $\rho > 0$ *is attracted to the homoclinic orbit on* $\rho = 0$.

Regarding part (e) of proposition 4.9, we observe numerically the existence of two numbers $\Delta_{\pm 0}$ such that

$$\delta_{-1} < \Delta_{-0} < -\nu < \Delta_0 < \Delta_1$$

and $W^c \equiv W^s$ for $\Delta = \Delta_{\pm 0}$ (cf. fig. 14b). For $\Delta \in (\delta_{-1}, \Delta_{-0}) \cup (\Delta_0, \Delta_1)$, the phase portraits are given in fig. 14a, and stable phase drift coexists with phase-locked saddle–nodes. Combining this with parts (a) and (b) of proposition 4.9 we have the coexistence of stable phase drift and phase-locked saddle–nodes for $\Delta \in (\delta_{-1}, \Delta_{-0}) \cup (\Delta_0, 2)$. As $\Delta \downarrow \Delta_0$ or $\Delta \uparrow \Delta_{-0}$, the limiting positions of the phase-drift solutions are the homoclinic orbits shown in fig. 14b. There are no phase-drift solutions when $\Delta = \Delta_{\pm 0}$ and the homoclinic orbits are semistable. The phase portraits for $\Delta \in (\Delta_{-0}, \Delta_0)$ are those in fig. 14c and there are no phase-drift solutions.

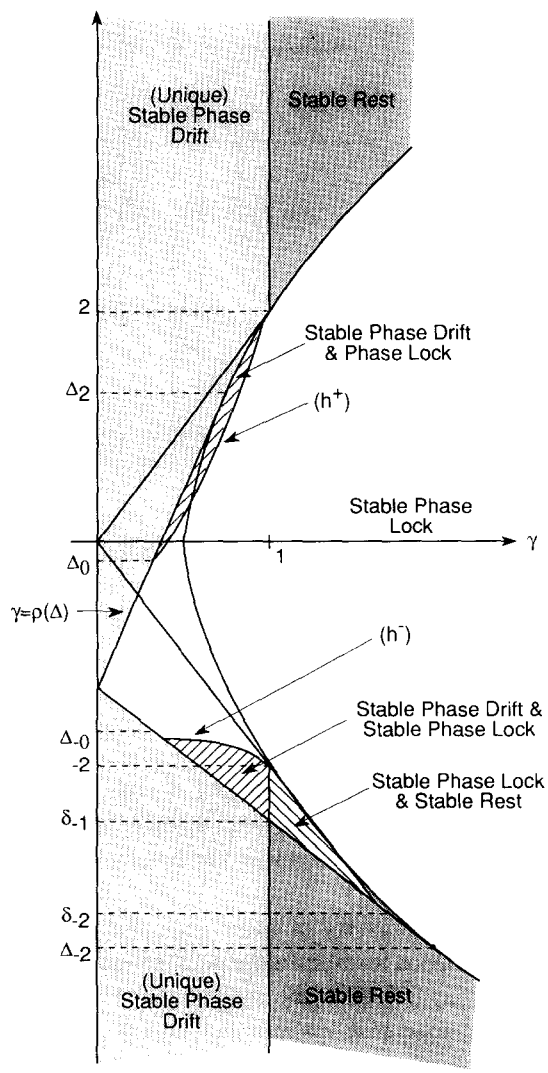

Fig. 15. Some numerically observed global bifurcations, specifically (h^+) and (h^-), which are discussed in the text.

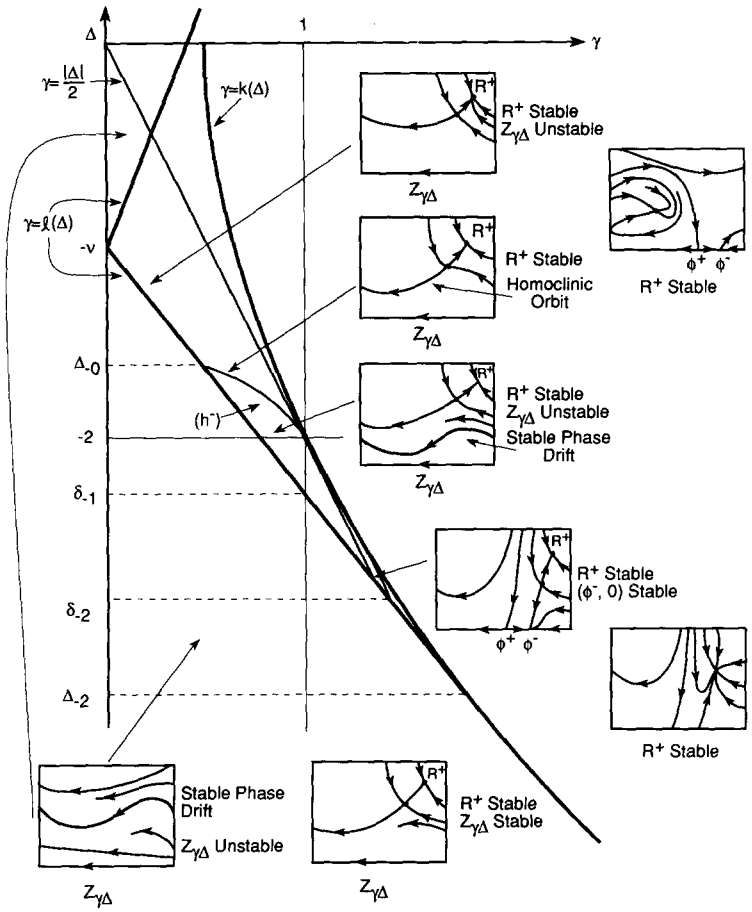

Fig. 16. A detailed picture of the various phase portraits in a neighborhood of (h^-). See text for description.

As γ increases from $p_\nu(\Delta)$ the saddle–node splits into a saddle point and a node, with the node always in the half-plane $\rho > 0$. By continuity, this phase-locked node will coexist with the stable phase-drift solution for $\Delta \in (\delta_{-1}, \Delta_0) \cup (\Delta_0, 2)$ and sufficiently small $\gamma > p_\nu(\Delta)$. In particular, for $\Delta \in (\delta_{-1}, \Delta_0) \cup (\Delta_0, \Delta_1)$ *the phase-locked node is stable, so there is coexistence of stable phase drift and stable phase lock for sufficiently small* $\gamma > p_\nu(\Delta)$. The boundaries of the parameter regions where phase drift and phase lock coexist are characterized by the occurrence of certain global bifurcations which we now describe.

There is a curve (h^-) extending from $(l(\Delta_{-0}), \Delta_{-0})$ to $(1, -2)$ along which there is a homoclinic connection formed by the coincidence of the stable and unstable manifolds of the R^- branch phase-locked saddle point. This curve is shown in figs. 15 and 16 and the corresponding phase portrait can be found in fig. 16. In fig. 16 we also show the phase portraits for various subregions of the parameter space near (h^-), but we have omitted the phase portraits for $\gamma = l_\nu(\Delta)$ since these are given in fig. 14. *For* (γ, Δ) *in the parameter region bounded by* (h^-), $\gamma = l_\nu(\Delta)$, *and* $\gamma = 1$, *stable phase lock and stable phase drift coexist as shown in the phase portrait in fig. 16.* As $\gamma \uparrow 1$ from inside this region, the phase-drift solution merges with the running solution $Z_{\gamma\Delta}$ and there is a transcritical (i.e. change of stability) bifurcation. In the region bounded by $\gamma = 1$, $\gamma = l(\Delta)$ and $\gamma = k(\Delta)$, the stable phase-locked solution coexists with either the stable running solution $Z_{\gamma\Delta}$ if $1 < \gamma < \frac{1}{2}|\Delta|$ or the stable node $(\phi^-, 0)$ if $\frac{1}{2}|\Delta| < \gamma < k(\Delta)$. For (γ, Δ) in the region

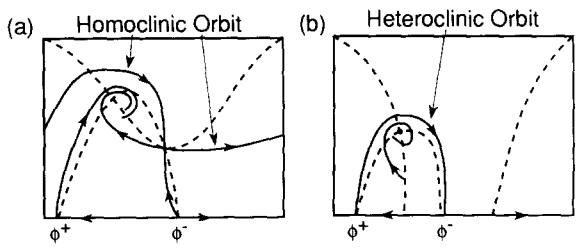

Fig. 17. Phase portraits on (h^+). (a) $\Delta_0 < \Delta < \delta^*$: there is a homoclinic orbit. (b) $\delta^* \leq \Delta < 2$: there is a heteroclinic orbit.

bounded by $\gamma = l_\nu(\Delta)$, $\gamma = \frac{1}{2}|\Delta|$ and (h^-), there is no phase drift and only the phase-locked solution is stable.

At $(l_\nu(\Delta_0), \Delta_0)$ there is a homoclinic connection for the saddle–node. There is also a curve (h^+) through $(l_\nu(\Delta_0), \Delta_0)$ to (1, 2) along which the homoclinic connection is extended (cf. fig. 15 and fig. 18). For Δ sufficiently close to Δ_0 the extension of this homoclinic connection is the coincidence of the stable and unstable manifolds of the saddle point (R^- branch) generated by the saddle–node (fig. 17a). As Δ increases the saddle point approaches the unstable node at $(\phi^-, 0)$ and they merge in a transcritical

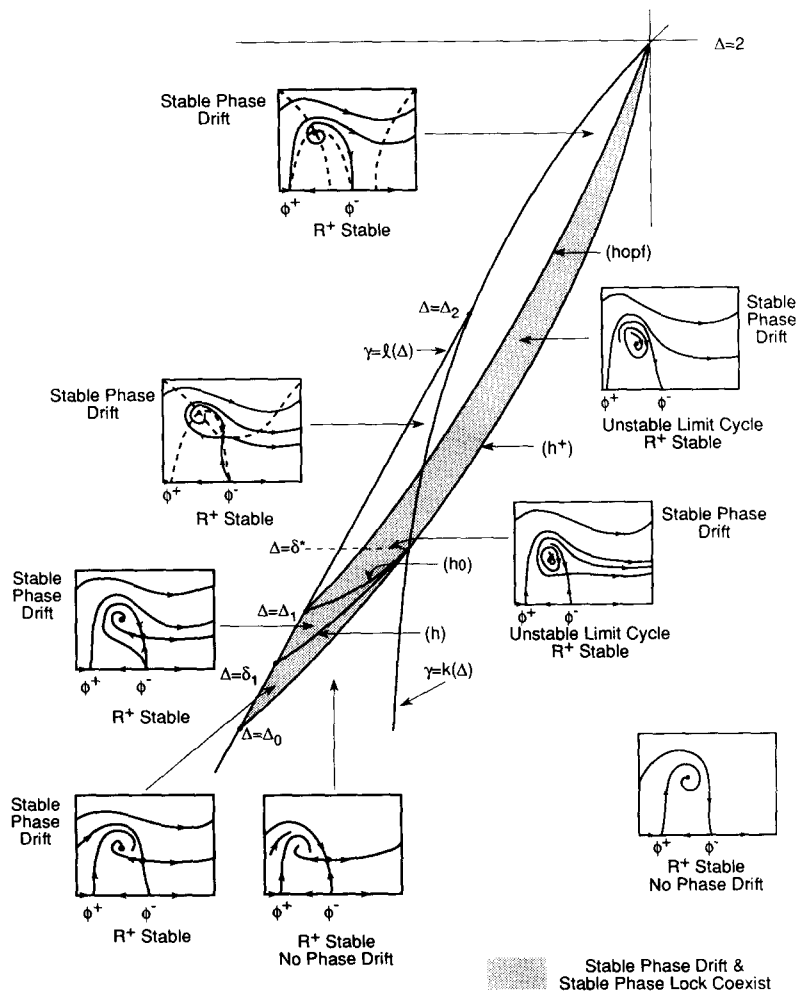

Fig. 18. A detailed picture of the various phase portraits in a neighborhood of (h^+). See text for description.

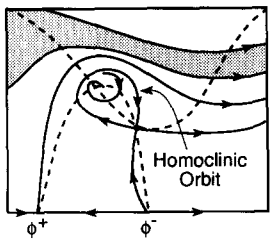

Fig. 19. Phase portrait on (ho), showing the homoclinic connection; $(\gamma, \Delta) \in$ (ho).

bifurcation at the point (k, δ^*) where (h^+) intersects $\gamma = k(\Delta)$. At this bifurcation the homoclinic connection becomes a heteroclinic connection in which the stable manifold of the saddle point at $(\phi^+, 0)$ and the unstable manifold of $(\phi^-, 0)$ coincide. This heteroclinic connection persists along (h^+) for $\Delta > \delta^*$ (fig. 17b) up to the point (1, 2).

Fig. 18 shows schematically an enlargement of the region S in the parameter space bounded by the curves $\gamma = p_\nu(\Delta)$ and (h^+). This region contains the Hopf bifurcation curve (hopf) given by (4.8) along which the R^+ branch of the phase-locked solutions becomes stable, as well as the two global bifurcation curves. One of these is the homoclinic connection curve (ho) which is associated with (hopf) in the unfolding of the Bogdanov–Takens point at (γ_1, Δ_1). Fig. 19 is the phase portrait for (γ, Δ) on (ho). To see how the other global bifurcation curve (labeled (h) in fig. 18) arises, observe that the phase portrait for $\gamma = l(\Delta)$ with sufficiently large $\Delta < \Delta_1$ is as shown in fig. 20a while the phase portrait for $\gamma = l(\Delta)$ with sufficiently small $\Delta > \Delta_0$ is as shown in fig. 20c. The transition between these two portraits occurs by means of the heteroclinic connection formed by the coincidence of the unstable manifold of the saddle point $(\phi^+, 0)$ and the stable manifold W^s of the saddle–node (fig. 20b). This configuration is observed to occur at a point $(l_\nu(\delta_1), \delta_1)$ with $\delta_1 \in (\Delta_0, \Delta_1)$. On the curve (h) emanating from $(l_\nu(\delta_1), \delta_1)$ this heteroclinic connection extends as the coincidence of the unstable manifold of $(\phi^+, 0)$ and the stable manifold of the R^- branch saddle point (fig. 21). The curves (h) and (ho) both terminate at (k, δ^*) (cf. fig. 18).

In fig. 18 we summarize the observed phase portraits near S and in the various subregions of S defined by the bifurcation curves (hopf), (ho) and (h). In the part of S which lies to the left of (hopf) the R^+

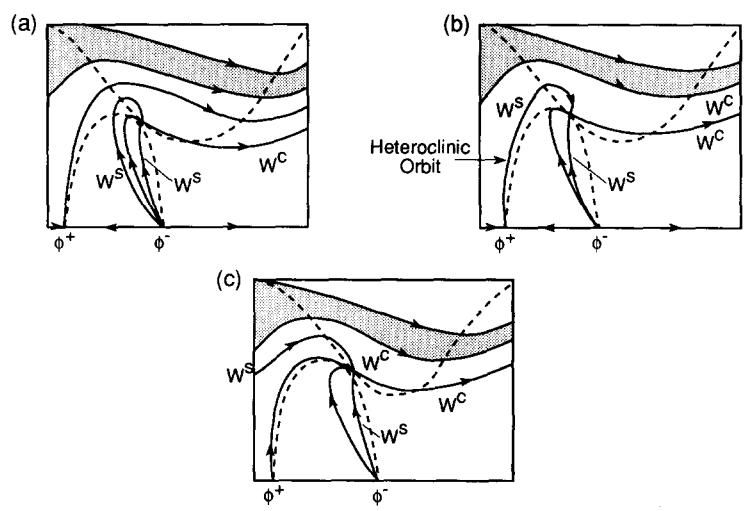

Fig. 20. Observed transitions on $\gamma = l(\Delta)$. (a) $\delta_1 < \Delta < \Delta_1$: W^s lies below $W^u(\phi^+, 0)$. (b) $\Delta = \delta_1$: $W^s = W^u(\phi^+, 0)$. (c) $\Delta_0 < \Delta < \delta_1$: W^s lies above $W^u(\phi^+, 0)$.

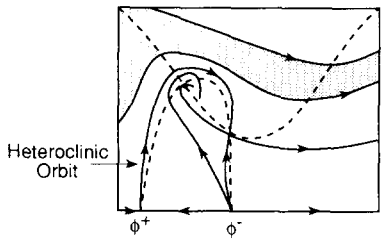

Fig. 21. The extension of the heteroclinic orbit shown in fig. 20b to points on (h).

branch phase-locked node is unstable. As the parameter point crosses (hopf) there is a Hopf bifurcation in which the R^+ branch phase-locked node becomes stable and spawns an unstable limit cycle (phase trap solution). This limit cycle is destroyed either in the homoclinic bifurcation on (ho) or in the heteroclinic bifurcation on (h^+) for $\Delta > \delta^*$. Note that although a stable phase-drift solution coexists with phase-locked solutions throughout S, there is a stable phase-locked solution only in the subregion of S bounded by the curves $\gamma = l_\nu(\Delta)$ for $\Delta \in [\Delta_0, \Delta_1]$, (hopf) and ($h^+$). This subregion where stable phase drift and stable phase lock coexist is shown shaded in fig. 18.

4.5. *Frequencies*

We now turn to a discussion of how the nature of the coupling (i.e. the value of κ) affects the frequency of the phase-locked solutions. For this, we need to have the equations in terms of the individual θ_i's instead of the phase difference ϕ. If we write eq. (2.1) in polar coordinates and set $r_1 = r_2 = r$ we obtain

$$\dot{r} = r(a - r^2) + \gamma\cos(\theta_2 - \theta_1),$$
$$\dot{\theta}_1 = \omega_1 + q_1(1 - r^2) + \gamma\sin(\theta_2 - \theta_1),$$
$$\dot{\theta}_2 = \omega_2 + q_2(1 - r^2) + \gamma\sin(\theta_1 - \theta_2),$$

where $a = 1 - \kappa\gamma$ for $\kappa \in [0,1]$. At phase lock, $r = \sqrt{R^\pm}$ and $\theta_2 - \theta_1 = \phi^\pm$, where the constants $R^\pm$ and $\phi^\pm$ are defined by (3.3). In particular, the right-hand sides of the θ-equations are constant, and it is not difficult to verify that

$$\theta_1^\pm(t) = f^\pm t + \theta_0, \qquad \theta_2^\pm(t) = f^\pm t + \theta_0 + \phi^\pm,$$

where the frequency $f^\pm$ is given by

$$f^\pm = \bar{\omega} + \bar{q}(1 - R^\pm)$$

with

$$\bar{\omega} = \tfrac{1}{2}(\omega_1 + \omega_2), \qquad \bar{q} = \tfrac{1}{2}(q_1 + q_2).$$

If $\nu \equiv q_1 - q_2 = 0$ then, according to (3.3),

$$R^\pm = a \pm \sqrt{\gamma^2 - \tfrac{1}{4}\Delta^2}$$

so that the symmetric phase-locked solutions are independent of the value of $\bar{q} = q_1 = q_2$. However, since

$$f^{\pm} = \bar{\omega} + \bar{q}\left(\kappa\gamma \mp \sqrt{\gamma^2 - \tfrac{1}{4}\Delta^2}\right)$$

the frequencies in general depend on $\bar{q}$. In particular, if $\bar{q} > 0$ then

$$\begin{aligned} f^+ &> \bar{\omega} \quad \text{for } \gamma < |\Delta|/2\sqrt{1-\kappa^2}, \\ &= \bar{\omega} \quad \text{for } \gamma = |\Delta|/2\sqrt{1-\kappa^2}, \\ &< \bar{\omega} \quad \text{for } \gamma > |\Delta|/2\sqrt{1-\kappa^2}, \end{aligned}$$

and if $\bar{q} < 0$ then

$$\begin{aligned} f^+ &< \bar{\omega} \quad \text{for } \gamma < |\Delta|/2\sqrt{1-\kappa^2}, \\ &= \bar{\omega} \quad \text{for } \gamma = |\Delta|/2\sqrt{1-\kappa^2}, \\ &> \bar{\omega} \quad \text{for } \gamma > |\Delta|/2\sqrt{1-\kappa^2}. \end{aligned}$$

For example, if $\bar{q} > 0$ then in the direct coupling case ($\kappa = 0$), $f^+ < \bar{\omega}$, while in the purely diffusive case ($\kappa = 1$), $f^+ > \bar{\omega}$.

5. Nonscalar coupling

The above descriptions concern behavior when the coupling between the oscillators is via a scalar matrix. The general nonscalar case, defined in complex coordinates by eqs. (A.5) and (A.6), cannot be analyzed using the methods of section 4. This is because we can no longer, in general, make any reductions in the order of the equations by using symmetry properties. Nevertheless, we can discern some interesting behavior of (A.5), (A.6) when the two oscillators are identical.

Torre [19] has shown that if two *identical* oscillators are coupled with diffusive and *scalar* coupling, the uniform in-phase oscillation is always asymptotically stable. We shall show that with nonscalar coupling, there are parameter regimes in which the in-phase and anti-phase solutions are simultaneously stable. There are also parameter regimes in which the anti-phase solution is the only stable one. Finally, we demonstrate the existence of Hopf bifurcations that can lead to stable phase-trapping (see section 1 for definition). We see none of the above phenomena when the coupling is scalar. Indeed, when the coupling is scalar and the oscillators are identical, then the in-phase solution is stable and the anti-phase solution is unstable, regardless of the presence or absence of shear.

The coupling we shall use is still not the most general; as in (A.10), we assume that $f_{12} = f_{22} \equiv \mu$. Also, we go back to the case $q_1 = q_2 \equiv q$ (i.e. shear is allowed, but not unequal shear, so the complications of the last section are avoided). The equations are then

$$\begin{aligned} \dot{r}_1 &= r_1\left(1 - \kappa\gamma - r_1^2\right) + r_2\left(\gamma\cos\phi - \mu\sin\phi\right), \\ \dot{r}_2 &= r_2\left(1 - \kappa\gamma - r_2^2\right) + r_1\left(\gamma\cos\phi + \mu\sin\phi\right), \\ \dot{\phi} &= q\left(r_1^2 - r_2^2\right) - \gamma\left(\frac{r_2}{r_1} + \frac{r_1}{r_2}\right)\sin\phi + \mu\left(\frac{r_1}{r_2} - \frac{r_2}{r_1}\right)\cos\phi. \end{aligned} \tag{5.1}$$

There are two symmetric solutions that are immediate, an in-phase solution and an out-of-phase solution. The in-phase solution satisfies

$$\rho^2 \equiv r_1^2 = r_2^2 = 1 + \gamma(1-\kappa), \quad \phi = 0, \tag{5.2}$$

independent of μ. Except for diffusive coupling ($\kappa = 1$), the amplitude of the coupled phase-locked system exceeds that of the individual uncoupled oscillators. The anti-phase or out-of-phase solutions satisfy

$$\rho^2 \equiv r_1^2 = r_2^2 = 1 - \gamma(1+\kappa), \quad \phi = \pi. \tag{5.3}$$

These solutions only exist for $\gamma < 1/(1+\kappa)$. They are smaller in amplitude than the in-phase and uncoupled oscillations.

To determine the stability, we linearize (5.1) about (5.2) and (5.3). The matrix of linearization is

$$J_1 = \begin{pmatrix} 1-\kappa\gamma-3\rho^2 & \pm\gamma & \mp\mu\rho \\ \pm\gamma & 1-\kappa\gamma-3\rho^2 & \pm\mu\rho \\ 2q\rho \pm 2\mu/\rho & 2q\rho \mp 2\mu/\rho & \mp 2\gamma \end{pmatrix}, \tag{5.4}$$

where we take the top sign for the in-phase and the bottom for the anti-phase solutions. If we let

$$P = \begin{pmatrix} 1 & 1 & 0 \\ 1 & -1 & 0 \\ 0 & 0 & 1 \end{pmatrix}$$

then $P^{-1}J_1P = J_2$, which has the same eigenvalues, is given by

$$J_2 = \begin{pmatrix} 1-\kappa\gamma-3\rho^2 \pm \gamma & 0 & 0 \\ 0 & 1-\kappa\gamma-3\rho^2 \mp \gamma & \mp\mu\rho \\ 0 & 4q\rho \pm 4\mu/\rho & \mp 2\gamma \end{pmatrix}. \tag{5.5}$$

(Note that J_2 is the Jacobian written in τ, σ, ϕ coordinates, and is related to the J of section 4.3 by a further interchange to σ, τ, ϕ coordinates. In each case, the coordinates are chosen to make it clear in which plane a certain Hopf bifurcation is taking place.) We can now show the following proposition.

Proposition 5.1

(A) The in-phase solution (5.2) is linearly asymptotically stable provided that

$$\gamma^2 + \mu^2 + (\mu q + \gamma)[(1-\kappa)\gamma + 1] > 0. \tag{5.6}$$

(B) The anti-phase solution (5.3) is linearly asymptotically stable provided that

$$\gamma < 1/(3+\kappa), \tag{5.7a}$$

$$\gamma^2 + \mu^2 + (\mu q + \gamma)[-1 + \gamma(1+\kappa)] > 0. \tag{5.7b}$$

Proof. Since (5.5) is block-diagonal with a one-dimensional and a two-dimensional block, the eigenvalues have negative real part if and only if the upper left entry is negative, the trace of the lower 2×2 matrix is

negative, and the determinant of the latter is positive. The first of these three conditions holds automatically for the in-phase solutions; using (5.2), it can be seen that the determinant is four times the expression in (5.6).

For the anti-phase solutions, (5.7a) is the requirement that the trace of the 2×2 matrix be negative; this is already strong enough to imply that the upper left-hand entry is negative. As in the case of the in-phase solutions, (5.7b) implies the determinant of the 2×2 matrix is positive. □

Proposition 5.1 implies that there are parameter regions in which the in-phase and the anti-phase solution are simultaneously stable. For example, we pick $q = 0$ and $\mu > 0$, so that (5.6) is always true. Next we pick γ small enough so that both (5.7a) and (5.7b) hold. For all γ less than this critical value, both the anti-phase and the in-phase solutions are stable. By continuity, this bistability holds for small frequency differences Δ; it crucially depends on μ being nonzero. We also note that for large coupling strengths (i.e. $\gamma > 1/(3 + \kappa)$) the anti-phase solution is never stable. If $\mu q < 0$, and $|\mu q|$ is sufficiently large, then (5.6) can fail while (5.7) holds. Thus, in that parameter regime, the anti-phase solution is stable and the in-phase solution is unstable.

Proposition 5.1 also enables us to see how stability is lost, and therefore to get information about the new types of solutions that emerge when the phase locked solutions become unstable. If the left-hand side of (5.6) becomes negative, then stability of the in-phase solution is lost through a zero eigenvalue. (The trace of the lower 2×2 matrix is negative and the determinant is zero when the left-hand side of (5.6) is zero.) It is easy to see that the derivative of the left-hand side of (5.6) with respect to γ, evaluated at that point, is not zero. It follows that the zero eigenvalue is a simple one, and that there is a new curve of stable critical points, not necessarily symmetric. (The usual additional hypotheses on the quadratic terms are required in order that there be an exchange of stability, with one stable solution for each γ in a neighborhood of the bifurcation point. In our case, these fail and there could be a pitchfork bifurcation, with two new stable solutions on one side, and none on the other.) That these new conditions are symmetric can be seen by noting that the bifurcation does not take place if we restrict ourselves to considering the space of symmetric solutions. (The eigenvector is in the plane $\tau = 0$, not $\sigma = 0$.) We note that if $\mu q \geq 0$, then (5.6) is always true and the in-phase solution is always stable. Thus, instability requires $\mu q < 0$, so for loss of stability to asymmetric phase-locked solutions, there must be both nonscalar coupling and "shear".

The two conditions (5.7a) and (5.7b) determine the stability of the anti-phase solution. If (5.7a) is violated but (5.7b) is true, then the trace of the 2×2 matrix vanishes with the determinent still positive; this implies the existence of a pair of complex conjugate eigenvalues. Again, it can be checked that the derivative of the trace with respect to γ is nonzero, so the eigenvalues cross the imaginary axis, i.e.. a Hopf bifurcation occurs. A numerically produced bifurcation diagram (fig. 22) shows that this bifurcation can be supercritical. We then have a new stable behavior, "phase trapping". (In section 4, we saw the existence of *unstable* phase-trapping, i.e., an unstable limit cycle in the plane of symmetric solutions. The phase-trapped solution of this section is not in the plane of symmetric solutions.) When (5.7b) is violated, but (5.7a) holds, a new asymmetric solution bifurcates from (4.3) near $\phi = \pi$ as for the in-phase solutions.

The behavior of this system is complicated in general. As an example of one of the more interesting bifurcation diagrams illustrating bistability, phase-trapping, and anti-symmetric phase locking, we offer fig. 22. Note that there are two stable phase-trap branches resulting from Hopf bifurcations on the stable asymmetric branches at $\gamma \approx 0.5$, and that these branches merge in a "gluing" bifurcation [30]. This diagram was determined numerically using AUTO and verified independently through another numerical method.

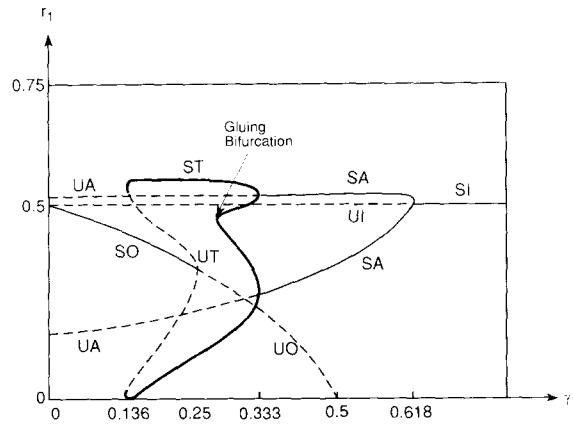

Fig. 22. Bifurcation diagram in $\gamma, \max r_1$ space for (5.1), with $\kappa = 1$, $\mu = 1$ and $q = 2$. SI represents stable in-phase locking, UI unstable in-phase locking. SA denotes stable, but asymmetric phase-locked solutions, UA unstable, asymmetric solution. ST stands for stable phase-trapping, UT for unstable phase trapping. In the trapped solution, the amplitude varies greatly, and the two branches labelled ST emerging from each SA, via a Hopf bifurcation, represent one phase-trapped solution. The two phase-trapped solutions merge to become one large solution. The phase-trapped solution disappears merging with the unstable phase-trapped solution in a saddle–node bifurcation. SO represents stable out-of-phase, or anti-phase solution, and UO the unstable out-of-phase solutions. Note that for γ small, the anti-phase solution is the only stable solution.

Some related work on pairs of identical oscillators are refs. [1, 11, 13, 15, 22, 23]. Numerical work was done by Screiber and Marek [22] on a pair of identical Brusselators, with coupling that was symmetric and diagonal, but nonscalar. They observed a variety of bifurcations to anti-phase oscillations, tori, and even chaotic behavior. Kawato and Suzuki [11] considered two coupled FitzHugh–Nagumo oscillators with nonscalar, and direct coupling. Unlike our analysis, which uses coupling strength as the main parameter, they use a measure of the distance of each (uncoupled) oscillator from a Hopf bifurcation. The bifurcation diagrams that they get are quite different from ours; in particular they do not get the asymmetric phase locked solutions. Rand and Holmes [15], studying coupled van der Pol oscillators, find regimes in which in-phase and anti-phase solutions are simultaneously stable, but no regime with only the anti-phase stable.

Acknowledgements

We wish to thank Professor E.J. Doedel for helpful conversations and computations.

Appendix

In this appendix we derive the various equations used in the body of the paper, e.g., eqs. (1.2). These equations arise from a fairly general class of linearly coupled oscillators each of which is near a Hopf bifurcation. We begin with the coupled systems

$$\begin{aligned} \mathrm{d}X_1/\mathrm{d}t &= \left(A + \tilde{\lambda} B_1\right) X_1 + N_1(X_1) + \tilde{\eta} D_1(X_2 - \tilde{\kappa}_1 X_1), \\ \mathrm{d}X_2/\mathrm{d}t &= \left(A + \tilde{\lambda} B_2\right) X_2 + N_2(X_2) + \tilde{\eta} D_2(X_1 - \tilde{\kappa}_2 X_2). \end{aligned} \tag{A.1}$$

X_1, X_2 are vectors in $\mathbb{R}^n$, A, B_j, and D_j are $n \times n$ real matrices, $\tilde{\lambda}$, $\tilde{\eta}$, and $\tilde{\kappa}_j$ are scalar parameters, and $N_j(X_j)$ are $\mathcal{O}(|X_j|^2)$ and C^3 smooth. The matrix A has a pair of imaginary eigenvalues and its remaining eigenvalues are in the left half complex plane. When $\tilde{\eta} = 0$ (no coupling), we assume that each of the uncoupled equations in (A.1) undergoes a stable supercritical Hopf bifurcation as $\tilde{\lambda}$ increases above zero. The matrices D_1, D_2 describe the coupling between the two weakly nonlinear oscillators and $\tilde{\eta}$ represents the strength of this coupling. The parameters $\tilde{\kappa}_j$ allow us to change from direct ($\tilde{\kappa}_j = 0$) to diffusive ($\tilde{\kappa}_j = 1$) coupling.

In order to ultimately derive eqs. (1.2) and others, we need to make some additional assumptions on eqs. (A.1), which we now spell out. In absence of coupling, we assume that the amplitudes and rates of attraction of the two stable oscillations are identical. Note that this does not imply that the isochrons or frequencies are necessarily the same. We will also assume that the coupling is symmetric so that $D_1 = D_2$ and $\tilde{\kappa}_1 = \tilde{\kappa}_2$. In the following, we will derive the most general bifurcation equations and then impose the above assumptions, whose consequences will become clear later.

It is known that in a Hopf bifurcation the smallest Floquet exponent of the periodic solution is proportional to the magnitude of $\tilde{\lambda}$, the deviation from criticality. Since we are concerned with the effects of coupling on the amplitudes of the two oscillators, we will assume that the coupling parameter $\tilde{\eta}$ and the bifurcation parameter $\tilde{\lambda}$ are of the same order of magnitude and both small. We also note that the amplitude of the periodic solution is proportional to the square root of $\tilde{\lambda}$. We shall scale the amplitude by ϵ, where $0 < \epsilon \ll 1$. Therefore, we scale $\tilde{\lambda}$ and $\tilde{\eta}$ by ϵ^2, i.e., we let

$$\tilde{\lambda} = \epsilon^2 \lambda \quad \text{and} \quad \tilde{\eta} = \epsilon^2 \eta. \tag{A.2}$$

Let $\pm i\omega_0$ be the imaginary eigenvalues of A, let $\Phi_0, \bar{\Phi}_0$ be the corresponding eigenvectors, and let $\Psi_0, \bar{\Psi}_0$ the corresponding eigenvectors for the adjoint matrix $-A^T$ satisfying $\langle \Psi_0, \Phi_0 \rangle = 1$. $\langle \Psi_0, \Phi_0 \rangle$ denotes the scalar product

$$\frac{\omega_0}{2\pi} \int_0^{2\pi/\omega_0} \bar{\Psi}_0(t) \cdot \Phi(t)\, dt.$$

We seek a solution to (A.1) of the form

$$X_j(t) = \epsilon \left[z_j(s) \Phi_0 e^{i\omega_0 t} + \bar{z}_j(s) \bar{\Phi}_0 e^{-i\omega_0 t} \right] + \epsilon^2 w_{j,2}(s,t) + \epsilon^3 w_{j,3}(s,t), \tag{A.3}$$

where $s = \epsilon^2 t$ is the slow time scale, $z_j(s)$ are complex scalar functions, and $w_{j,2}$, $w_{j,3}$, etc. are terms orthogonal to the space generated by the real imaginary parts of $\Phi_0 e^{i\omega_0 t}$. (A.3) is inserted in (A.1), producing an equation for each order of ϵ. At $\mathcal{O}(\epsilon)$, we obtain an identity. At $\mathcal{O}(\epsilon^2)$, there is an equation for $w_{j,2}$. This equation has the form $(d/dt - A) w_{j,2} = g_2$, where g_2 depends on A and the quadratic terms of $N_j(X_j)$. Such an equation has a unique periodic solution if and only if $\langle \Psi_0, g_2 \rangle = 0$. It is easily checked that g_2 has no terms of the form $e^{\pm i\omega t}$, and hence g_2 is orthogonal to $\Psi_0, \bar{\Psi}_0$. It follows that the $\mathcal{O}(\epsilon^2)$ equations can be solved for $w_{j,2}$. At $\mathcal{O}(\epsilon^3)$, there are terms of the form $e^{\pm i\omega t}$ which must vanish in order that there be a periodic $w_{j,3}$. The vanishing condition gives rise to the equation.

$$\partial z_j / \partial s = z_j \left[\lambda (a_j + i b_j) - (p_j + i\tilde{q}_j) z_j \bar{z}_j \right] + \eta (d_{j1} + i d_{j2})(z_k - \tilde{\kappa}_j z_j), \qquad j,k = 1,2, \quad j \neq k. \tag{A.4}$$

The parameters a_j, b_j, p_j, and q_j are real. The complex scalar $p_j + i\tilde{q}_j$ depends only on A and the

nonlinear functions $N_j(X_j)$ and

$$a_j + \mathrm{i}b_j = \langle \Psi_0, B_j \Phi_0 \rangle.$$

The assumption that the Hopf bifurcation is supercritical and stable implies that a_j and p_j are both positive. The diffusion matrix D_j gives rise to the term

$$d_{j1} + \mathrm{i}d_{j2} = \langle \Psi_0, D_j \Phi_0 \rangle.$$

Eq. (A.4) has an invariance under rotation, i.e., $z \to \mathrm{e}^{\mathrm{i}\alpha} z$, $\alpha \in \mathbb{R}$. To exploit this we shall rewrite (A.4) in scaled polar coordinates, also introducing a scaled time $\tau = \lambda a_1 s$. See ref. [31] for related work. Let

$$z_j = \sqrt{\lambda a_j / p_j}\, r_j \mathrm{e}^{\mathrm{i}\theta_j}.$$

These new variables satisfy

$$\begin{aligned}
\dot{r}_1 &= r_1(1 - r_1^2) + f_{11}[r_2 \cos(\theta_2 - \theta_1) - \kappa_1 r_1] - f_{12} r_2 \sin(\theta_2 - \theta_1), \\
\dot{r}_2 &= a r_2(1 - r_2^2) + f_{21}[r_1 \cos(\theta_1 - \theta_2) - \kappa_2 r_2] - f_{22} r_1 \sin(\theta_1 - \theta_2), \\
\dot{\theta}_1 &= \omega_1 + q_1(1 - r_1^2) + \frac{r_2}{r_1}[f_{11} \sin(\theta_2 - \theta_1) + f_{12} \cos(\theta_2 - \theta_1)] - f_{12}\kappa_1, \\
\dot{\theta}_2 &= \omega_2 + q_2(1 - r_2^2) + \frac{r_1}{r_2}[f_{21} \sin(\theta_1 - \theta_2) + f_{22} \cos(\theta_1 - \theta_2)] - f_{22}\kappa_2,
\end{aligned} \tag{A.5}$$

where,

$$a = a_2/a_1, \qquad q_j = a_j \tilde{q}_j / p_j a_1, \qquad \omega_j = b_j/a_1 - q_j,$$

$$\kappa_j = \tilde{\kappa}_j \sqrt{p_2 a_1 / p_1 a_2}, \qquad f_{1j} = \frac{\eta d_{1j} \sqrt{p_1 a_2 / p_2 a_1}}{\lambda a_1}, \qquad f_{2j} = \frac{\eta d_{2j} \sqrt{p_2 a_1 / p_1 a_2}}{\lambda a_1}.$$

A rigorous statement about the above derivation is as follows: there is a four-dimensional subspace invariant under (A.1) that exists because of the Hopf bifurcations; it is the center manifold for (A.1). Suppose that the parameters are scaled as in (A.2) and let $X_j = \epsilon Y_j$. Let $\bar{\theta}_j$, r_j be polar coordinates for the two-dimensional center manifold for each uncoupled oscillator, with the amplitude scaled like Y_j. Then there is an almost identity change of polar coordinates on the four-dimensional center manifold such that, up through terms of order $\mathcal{O}(\epsilon^2)$ and using the scaled time $s = \epsilon^2 t$, the equations for r_j, $\theta_j \equiv \bar{\theta}_j - \omega_0 t$ can be written in the form (A.5). From this it can be concluded by the usual arguments that any structurally stable feature of (A.5), such as a stable critical point or limit cycle, persists for the full system for ϵ sufficiently small.

It is not computationally efficient to derive (A.5) in this manner. However, we sketch the ideas below; the details may be supplied by the reader. It is simplest conceptually to do the almost identity change of coordinates in two steps. The first puts each oscillator into normal form up through $\mathcal{O}(\epsilon^2)$. That is, there is an almost identity change of coordinates for each uncoupled oscillator such that its equations have the form [32]

$$\begin{aligned}
\mathrm{d}\bar{\theta}_j/\mathrm{d}t &= \omega_0 + \epsilon^2 \omega_1 + \epsilon^2 (A_j - B_j r_j^2) + \mathcal{O}(\epsilon^3) \equiv \omega_0 + \epsilon^2 F(r_j, \epsilon), \\
\mathrm{d}r_j/\mathrm{d}t &= \epsilon^2 (C_j - D_j r^2) + \mathcal{O}(\epsilon^3) \equiv \epsilon^2 G(r_j, \epsilon).
\end{aligned} \tag{A.6}$$

In these coordinates, the coupled system has the form

$$\begin{aligned} \mathrm{d}\bar{\theta}_j/\mathrm{d}t &= \omega_0 + \epsilon^2 F(r_j, \epsilon) + \epsilon^2\left(\frac{r_k}{r_j} h_{jk}(\bar{\theta}_j, \bar{\theta}_k) + \bar{h}_j(\bar{\theta}_j)\right) + \mathcal{O}(\epsilon^3), \\ \mathrm{d}r_j/\mathrm{d}t &= \epsilon^2 G(r_j, \epsilon) + \epsilon^2\left[r_j K_{jj}(\bar{\theta}_j, \bar{\theta}_k) + r_k K_{jk}(\bar{\theta}_j, \bar{\theta}_k)\right] + \mathcal{O}(\epsilon^3), \end{aligned} \tag{A.7}$$

$j, k = 1, 2$, $j \neq k$. We now introduce $\phi \equiv \bar{\theta}_2 - \bar{\theta}_1$ and substitute $\bar{\theta}_1 + \phi$ for $\bar{\theta}_2$ in the equation for $\mathrm{d}\bar{\theta}_1/\mathrm{d}t$ and $\bar{\theta}_2 - \phi$ for $\bar{\theta}_1$ in the equation for $\mathrm{d}\bar{\theta}_2/\mathrm{d}t$. Since $\mathrm{d}\phi/\mathrm{d}t = \mathcal{O}(\epsilon^2)$, standard averaging theory [33] then allows an almost identity change of variables for $\bar{\theta}_1$ and $\bar{\theta}_2$ such that, in the new coordinates, the functions $h_{jk}(\bar{\theta}_j, \bar{\theta}_k)$ and $\bar{h}_j(\bar{\theta}_j)$ are replaced up through $\mathcal{O}(\epsilon^2)$ by their averages over $\bar{\theta}_j$; the first such average depends only on ϕ and the second is a constant. Changing to the s time scale and using the variables θ_j instead of $\bar{\theta}_j$, we get equations of the form (A.5). We leave to the reader to check that the coefficients are the same as derived in the first manner. A similar computation was done in ref. [8].

Finally, to derive eqs. (1.2) and the other equations in the body of this paper, we use the assumptions laid out in the beginning of this appendix. The equality of amplitudes and rates of attraction of the limit cycles implies that $a_1 = a_2$ and $p_1 = p_2$. If the coupling is symmetric then $\kappa_1 = \kappa_2 = \kappa$, $f_{11} = f_{21} = \gamma$, and $f_{12} = f_{22} = \mu$. If we let $\phi = \theta_2 - \theta_1$ denote the phase difference, then (A.5) becomes a third-order differential equation:

$$\begin{aligned} \dot{r}_1 &= r_1(1 - \kappa\gamma - r_1^2) + \gamma r_2 \cos\phi - \mu r_2 \sin\phi, \\ \dot{r}_2 &= r_2(1 - \kappa\gamma - r_2^2) + \gamma r_1 \cos\phi + \mu r_1 \sin\phi, \\ \dot{\phi} &= \Delta + q_1 r_1^2 - q_2 r_2^2 - \gamma \sin\phi\left(\frac{r_2}{r_1} + \frac{r_1}{r_2}\right) + \mu \cos\phi\left(\frac{r_1}{r_2} - \frac{r_2}{r_1}\right), \end{aligned} \tag{A.8}$$

where $\Delta = (\omega_2 - \omega_1) + (q_2 - q_1)$. If the original coupling matrices D_j are scalar, then $d_{j2} = 0$, so that $\mu = 0$ and we have eq. (1.2).

Remarks

(1) We have seen that equal attractivity and amplitude of the uncoupled oscillators allows us to assume with no loss in generality that $\lambda a_j = p_j = 1$. Furthermore, scalar symmetric coupling implies that $d_{j2} = 0$, $\tilde{\kappa}_1 = \tilde{\kappa}_2$, and $\eta d_{11} = \eta d_{21} = \gamma$. Substituting these into (A.4) yields (2.1).

(2) Eq. (A.8) is similar to one studied by Chakraborty and Rand [24]. The model they study arises when two van der Pol oscillators are coupled via an inductor. Their equations are (A.8) with $\gamma = 0$, $\kappa = 1$ and $q_1 = q_2 = 0$. Our paper is primarily concerned with the case $\gamma \neq 0$ so that our results complement those of the above authors. We also consider the behavior with "twist", $q_j \neq 0$, which is not studied in ref. [24].

(3) Recently, Aronson et al. [1] have extensively analyzed a system similar to the model considered in this paper. To compare the two models, we return to eq. (A.5) under the assumptions made in the appendix (equal amplitude and stability of the uncoupled oscillators as well as symmetric coupling). We rewrite these equations in rectangular form by introducing the variables $(u_j, v_j) = r_j(\cos\theta_j, \sin\theta_j)$:

$$\begin{aligned} \dot{u}_1 &= \lambda_1 u_1 - \Omega_1 v_1 + \gamma(u_2 - \kappa u_1) - \mu(v_2 - \kappa v_1), \\ \dot{v}_1 &= \lambda_1 v_1 + \Omega_1 u_1 + \mu(u_2 - \kappa u_1) + \gamma(v_2 - \kappa v_1), \\ \dot{u}_2 &= \lambda_2 u_2 - \Omega_2 v_2 + \gamma(u_1 - \kappa u_2) - \mu(v_1 - \kappa v_2), \\ \dot{v}_2 &= \lambda_2 v_2 + \Omega_2 u_2 + \gamma(v_1 - \kappa v_2) + \mu(u_1 - \kappa u_2), \end{aligned} \tag{A.9}$$

where

$$\lambda_j = 1 - u_j^2 - v_j^2, \quad \Omega_j = \omega_j + q_j\left(1 - u_j^2 - v_j^2\right).$$

In ref. [1], the following equation is considered:

$$\begin{aligned}
\dot{u}_1 &= \tilde{\lambda}_1 u_1 - \tilde{\Omega}_1 v_1 + \gamma(u_2 - u_1) + \gamma(v_2 - v_1),\\
\dot{v}_1 &= \tilde{\lambda}_1 v_1 + \tilde{\Omega}_1 u_1 + \gamma(v_2 - v_1) + \gamma(u_2 - u_1),\\
\dot{u}_2 &= \tilde{\lambda}_2 u_2 - \tilde{\Omega}_2 v_2 + \gamma(u_1 - u_2) + \gamma(v_1 - v_2),\\
\dot{v}_2 &= \tilde{\lambda}_2 v_2 + \tilde{\Omega}_2 u_2 + \gamma(v_1 - v_2) + \gamma(u_1 - u_2),
\end{aligned}$$

where $\tilde{\lambda}_j = \lambda_j$, and $\tilde{\Omega}_j = \omega$. They restrict their analysis to the "no-shear" case and study the implications of an effective diffusion matrix of the form

$$\gamma\begin{pmatrix} 1 & 1 \\ 1 & 1 \end{pmatrix},$$

while the diffusion matrix in (A.9) is of the form

$$\begin{pmatrix} \gamma & -\mu \\ \mu & \gamma \end{pmatrix}. \tag{A.10}$$

The model in ref. [1] is not a subcase of even the most general form, (A.5), since the coupling we assume always reduces to (A.10) when $\kappa_j = 0$ (although the values of μ and γ could be different for the two oscillators if coupling is not symmetric or if the oscillators have different amplitudes or stability properties.) Our particular choice of diffusion matrices allows us to reduce the fourth-order equation to a third-order one, which considerably simplifies the analysis. We do not obtain the complex resonance structures and period-doubling behavior found in their paper, but many of the other features are seen in (A.8) and (A.9) in a more transparent fashion.

Note added in proof

It has come to our attention that an earlier reference to a phenomenon similar to what we refer to here as the "Bar-Eli effect" is in ref. [34]. That paper dealt in a formal manner with a large population of oscillators having a spread of natural frequencies. Two recent papers [35, 36] have extended the work on oscillator death to $N \gg 1$ oscillators each coupled to every other oscillator.

References

[1] D.G. Aronson, E.J. Doedel and H.G. Othmer, An analytical and numerical study of the bifurcations in a system of linearly coupled oscillators, Physica D 25 (1987) 20–104.
[2] S. Baer and C. Tier, An analysis of a dendritic neuron with an active membrane site, J.Math. Biol. 23 (1986) 137–161.
[3] K. Bar-Eli, On the stability of coupled chemical oscillators, Physica D 14 (1985) 242–252.
[4] S. Daan and C. Berde, Two coupled oscillators; simulations of the circadian pacemaker in mammalian activity rhythms, J. Theor. Biol. 70 (1978) 297–314.

[5] G.B. Ermentrout, $n:m$ phase locking of weakly coupled oscillators, J. Math. Biol. 12 (1981) 326–342.
[6] G.B. Ermentrout, The behavior of rings of coupled oscillators, J. Math. Biol. 23 (1985) 55–74.
[7] G.B. Ermentrout, Losing amplitude and saving phase, in: Nonlinear Oscillations in Biology and Chemistry, H.G. Othmer, ed., Springer Lecture Notes in Biomathematics, Vol. 66 (Springer, Berlin, 1986).
[8] G.B. Ermentrout and N. Kopell, Frequency plateaus in a chain of weakly coupled oscillators I, SIAM J. Math. Anal. 15 (1984) 215–237.
[9] G.B. Ermentrout and J. Rinzel, Beyond a pacemaker's entrainment limit: phase walk-through, Am. J. Physiol. 246 (1984) R102–R106.
[10] F.C. Hoppensteadt and J.P. Keener, Phase locking of biological clocks, J. Math. Biol. 15 (1982) 339–349.
[11] M. Kawato and R. Suzuki, Two coupled neural oscillators as a model of the circadian pacemaker, J. Theor. Biol. 86 (1980) 547–575.
[12] N. Kopell and G.B. Ermentrout, Symmetry and phase locking in chains of weakly coupled oscillators, Comm. Pure. Appl. Math. 39 (1986) 623–660.
[13] D.A. Linkens, The stability of entrainment conditions for RLC coupled van der Pol oscillators used as a model for intestinal electrical rhythms, Bull. Math. Biol. 39 (1977) 359–372.
[14] J.C. Neu, Coupled chemical oscillators, SIAM J. Appl. Math. 37 (1979) 307–315.
[15] R.H. Rand and P.J. Holmes, Bifurcation of periodic motions in two weakly coupled van der Pol oscillators, Int. J. Nonlin. Mech. 15 (1980) 387–399.
[16] A.H. Cohen, P.J. Holmes and R.H. Rand, The nature of coupling between segmental oscillators of the lamprey spinal generator, J. Math. Biol. 13 (1982) 345–369.
[17] M.St. Vincent, Entrainment of a limit cycle oscillator with shear by large amplitude forcing, SIAM J. Appl. Math. 19 (1988) 648–666.
[18] S. Smale, A mathematical model of two cells via Turing's equation, Some Mathematical Questions in Biology V, Lectures on Mathematics in the Life Sciences, No. 6 (Am. Math. Soc., Providence, RI, 1974) pp. 17–26.
[19] V. Torre, A theory of synchronization of two heart pace-maker cells, J. Theor. Biol. 61 (1976) 55–71.
[20] A.T. Winfree, The Geometry of Biological Time (Springer, Berlin, 1980).
[21] N. Fenichel, Persistence and smoothness of invariant manifolds for flows, Ind. Univ. Math. J. 21 (1971) 193–226.
[22] I. Schreiber and M. Marek, Strange attractors in coupled reaction-diffusion cells, Physica D 15 (1982) 258–292.
[23] P. Holmes and R. Rand, Bifurcations of the forced van der Pol oscillator, Quart. Appl. Math. 35 (1978) 495–509.
[24] T. Chakraborty and R. Rand, The transition from phase locking to drift in a system of two weakly coupled van der Pol oscillators, Int. J. Nonlin. Mech. 23 (1988) 369–376.
[25] A.M. Turing, The chemical basis for morphogenesis, Phil. Trans. R. Soc. London Ser. B 237 (1952) 37–72.
[26] G.B. Ermentrout and N. Kopell, Oscillator death in systems of coupled oscillators, SIAM J. Appl. Math., to appear.
[27] M. Crowley and I. Epstein, Experimental and theoretical studies of a coupled chemical oscillator: phase death, multistability and in- and out-of-phase entrainment, J. Phys. Chem. 93 (1989) 2496–2502.
[28] J. Guckenheimer and P. Holmes, Nonlinear Oscillations, Dynamical Systems, and Bifurcations of Vector Fields (Springer, Berlin 1983).
[29] J. Hale, Ordinary Differential Equations (Wiley–Interscience, New York, 1969).
[30] J.M. Gambaudo, P. Glendinning and C. Tresser, The gluing bifurcation I. Symbolic dynamics of the closed curves, Nonlinearity 1 (1988) 203–213.
[31] D.H. Sattinger, Group Theoretic Methods in Bifurcation Theory, Lecture Notes in Mathematics, Vol. 762 (Springer, Berlin, 1970).
[32] S.-N. Chow and J. Mallet-Paret, Integral averaging and bifurcation, J. Diff. Eqs. 26 (1977) 112–159.
[33] S.-N. Chow and J. Hale, Methods of Bifurcation Theory (Springer, Berlin, 1982).
[34] Y. Yamaguchi and H. Shimizu, Theory of self-organization in the presence of native frequency distributions and external noise, Physica D 11 (1984) 212–226.
[35] G.B. Ermentrout, Oscillator death in populations of "all to all" coupled nonlinear oscillators, Physica D 41 (1990) 219–231.
[36] R. Mirollo and S. Strogatz, Amplitude death in an array of limit cycle oscillators, preprint.